Charles University in Prague
Faculty of Science

Photogeneration of charge carriers in substituted polyacetylenes

Fotogenerace nosičů náboje v substituovaných polyacetylenech

Author: Michal Jex
Study programme: Chemistry
Branch of study: Physical chemistry
Supervisor: RNDr. Jiří Pfleger, CSc.
Consultants: Mgr. Miroslav Menšík, Dr.; RNDr. Petr Toman, Ph.D.
Academic year: 2012/2013

Acknowledgement
I would like to thank my supervisor RNDr. Jiří Pfleger, CSc. for suggesting the topic of my thesis, all the help, patience and countless hours of consultations. I would also like to thank my consultants Mgr. Miroslav Menšík, Dr. and RNDr. Petr Toman, Ph.D. for all the help and ideas how to improve my thesis.

Prohlášení
Prohlašuji, že jsem tuto závěrečnou práci zpracoval samostatně a že jsem uvedl všechny použité informační zdroje a literaturu. Tato práce ani její podstatná část nebyla předložena k získání jiného nebo stejného akademického titulu.

V Praze dne 20.května 2013

Michal Jex

Abstract
We present an improved model of charge carrier photogeneration in π-conjugated polymers with weak intermolecular interactions based on the model of Arkhipov. It includes quantum effects affecting the creation of charge transfer states, which occurs as an intermediate step in the free charge carrier photogeneration process. The electrostatic potential between the electron and the hole and transfer integrals needed for the calculation of the potential barrier for the charge transfer state dissociation are calculated quantum-chemically. We apply our model on experimental data of the charge carrier photogeneration efficiency in poly[1-trimethylsilylphenyl,2-phenyl]acetylene to explain its dependence on applied electric field. We eliminate several problems of the previous model. We are able to fit experimental data with just one set of parameters in the whole interval of the applied electric field. We do not have to consider several intervals of the electric field separately as in the previous work and reduce the number of needed parameters to three.

Key words
π-conjugated polymers, charge carrier photogeneration, photoconductivity

Abstrakt
Analyzujeme námi navržený model fotogenerace volných nosičů náboje v π-konjugovaných polymerních materiálech se slabými mezimolekulárními interakcemi vycházející z Archipovova modelu. Zahrnuli jsme kvantové efekty ovlivňující vznik stavů spojených s přenosem náboje představující mezikrok při fotogeneraci volných nosičů náboje. Elektrostatická interakce mezi elektronem a dírou, stejně tak jako přenosové integrály, jsou spočteny kvantověchemicky. Model jsme aplikovali na experimentální data závislosti fotogenerace volných nosičů náboje v poly[1-trimethylsilylfenyl,2-fenyl]acetylenu na intenzitě vnějšího elektrického pole. Podařilo se odstranit některé nedostatky předchozího modelu. Byli jsme schopni namodelovat experimentální data bez nutnosti rozdělení intervalu intenzit elektrických polí na několik oblastí, ve kterých bylo nutno prokládat experimentalní data modelovými křivkami s různými fyzikalními parametry. Náš model je schopen popsat experimentální data v celém rozsahu intenzit elektrického pole pomocí jedné sady parametrů modelu. Dále se nám podařilo snížit počet parametrů modelu na tři.

Klíčová slova
π-konjugované polymery, fotogenerace nosičů náboje, fotovodivost

Contents

List of used symbols

A	preexponential factor
A_{eff}	effective preexponential factor
d	initial separation distance
d_{min}	minimal distance between the trap and the polymer backbone
D	diffusion coefficient
ΔE	height of the potential barrier
e	elementary charge
$\mathbf{E}$	matrix of the potential well in the site basis
E_k	kinetic energy of the particle
E_{max}	local maximum of the electric potential energy
E_{min}	minimal energy of the hole
E_{minim}	local minimum of the potential well
E_1, E_2	energy of the highest occupied molecular orbital of the first and the second monomer unit
E_+	energy of the highest occupied molecular orbital of the dimer
E_-	energy of the second highest occupied molecular orbital of the dimer
ϵ	permittivity of the material
ϵ_r	relative permittivity of the material
ϵ_0	permittivity of the vacuum
η	total quantum yield
η_{eff}	primary effective quantum yield
η_0	primary quantum yield
$f(F, r, \theta)$	probability that the hole-electron pair do not recombinate
F	absolute value of the external electric field
$\overrightarrow{F}$	external electric field
$g(r, \theta)$	initial space distribution of the thermalized pairs
γ	inverse localization length
h	Planck constant
$\hbar$	reduced Planck constant
H	Hamiltonian of the molecule
H_{el}	electron Hamiltonian
k	Boltzmann constant
$k(\theta)$	probability of the bound state creation
k_{AI}	rate constant of autoinonization
k_{esc}	rate of CT state dissociation

k_E	rate constant of the exciton creation
k_g^{CT}	rate constant of CT state relaxation into the ground state
k_g^{EX}	rate constant of exciton recombination
k_i	rate constant of loss channels
k_n	rate constant of non-radiative transitions
k_r	rate constant of radiative transitions
k_{rec}	rate constant of CT state recombination
k_{rec}^{eff}	effective rate constant of CT state recombination
k_1	rate constant of transition of the exciton to the CT state
k_{-1}	rate constant of transition of the CT state to the exciton
K	recombination rate
m_e	mass of the electron
m_{eff}	effective mass of the hole
M_j	mass of the j-th atom
N_d	concentration of the electron acceptors
ν_e	frequency factor
ν_{esc}	rate of the CT state recombination
ν_{ph}	phonon frequency
ν_{rec}	rate of the CT state recombination
ν_0	frequency factor
ω	oscillation frequency
Ω	dissociation probability of a bound pair
$p(r)$	Gaussian distribution of thermalization distances
p_{esc}	probability of CT state dissociation
$P(d)$	Poisson distribution of the electron acceptors
Φ_{abs}	rate of photon absorbtion per unit volume
r_m	mean lowest intramolecular distance
r_{min}	location of the potential minimum
r_0	thermalization distance
σ	dispersion of the thermalization distance in the Ballistic model
T	temperature
$\mathcal{T}$	transfer integral
τ	mean lifetime of the exciton
τ_i	ionization time
τ_r	recombination time
τ_{th}	thermalization time
U	electric potential energy

$\mathcal{U}_e$	electric potential of the anion radical
U_{max}	local maximum of the energy
U_{osc}	second order Taylor expansion of U around r_{min}
$w(d, z)$	probability of creation of free charge carriers after one photon absorbtion
w_d	probability of the exciton dissociation
Z_j	charge of the j-th atom nucleus

List of used abbreviations

CT state	charge transfer state
HF method	Hartree-Fock method
DFT	density functional theory
DFT method	DFT method with the hybrid functional B3LYP in the atomic orbital basis 6-31G*
DFTD method	DFT method with the hybrid functional B3LYP in the atomic orbital basis 6-31G* with added dispersion

Chapter 1

Introduction

In this work we study photogeneration of free charge carriers in poly[1-trimethylsilylphenyl,2-phenyl]acetylene, which is an example of one dimensional organic semiconductor. Poly[1-trimethylsilylphenyl,2-phenyl]acetylene is an example of a polymer with well separated π-conjugated system on the polymer backbone. We further generalize Arkhipov model first presented in [1] and revisited in [2, 3]. We take into consideration several quantum effects which were either neglected in the previous models or approximated using classical methods.

The reason for studying the photogeneration of free charge carriers is the following: it is a principal process in photovoltaic cells, photoelectric sensors and xerographic photosensitive layers. The photogeneration as well as the transport of free charge carriers follows different mechanism as compared to inorganic semiconductors. Unlike the inorganic compounds, we are not able to describe this process within the energy band structure of the material. The reason for this is a weaker interaction between the molecules in organic compounds which leads to energy bands too narrow to be able to explain the photogeneration of free charge carriers and the conductivity of the material. Another difference might be observed in dielectric constant: in inorganic semiconductors its value usually exceeds 10 but in organic materials its value is around 3. Due to the smaller values of the dielectric constant in organic materials the mutual Coulomb attraction force in an electron-hole pair is much stronger. After the photoexcitation of the organic semiconductive materials an exciton is created as a primary quasiparticle instead of a free electron and a hole. The exciton is essentially the pair of electron and

hole bounded mutually by Coulomb attraction. After the creation of the electron-hole pair further activation energy is needed for the creation of free charge carriers. This process was previously a topic for a number of scientific investigations.

In Chapter 2 we summarize several previously developed models used for the description of the photogeneration of free charge carries in organic materials along with the essential basics of ab initio chemical calculations.

Chapter 3 is focused on molecular structure of our polymer. By means of density functional theory we calculated the structure and the geometry of the decamer model of our polymer. We present an optimization of the geometry of the neutral molecule and ion-radicals. We show a basic approach of calculating the position of the cation-radical and the anion-radical with respect to each other. Spin densities and charge distribution were calculated, too.

In Chapter 4 we present our improvements of the Arkhipov model of photogeneration of free charge carriers. The interaction between the anion-radical and a test charge was calculated. We showed the calculated transfer integral between the neighbor monomer units dependence on the dihedral angle between them. A detail analysis of the calculation of the potential barrier is given.

Chapter 2

Theoretical background

In this chapter we summarize existing models of photogeneration of free charge carriers in organic compounds. We introduce a modified Arkhipov model, which we improve later on. Some essential basics connected with ab initio quantum calculation are given at the end of this chapter.

2.1 Photogeneration of free charge carriers in organic compounds

First models explaining the formation of free charge carriers upon photoexcitation were developed to describe photoconductivity in organic molecular crystals. According to [4] the photogeneration of free charge carriers in organic compounds is connected, first, with the formation of an exciton after photoexcitation and, in the second step, with a subsequent dissociation of this exciton into free charge carriers. The exciton can be described as a bound state of the electron and the hole attracted to each other by the Coulomb force. The dissociation of the exciton is a thermally activated process. In conjugated polymers the concept of intrachain and interchain exciton is frequently used. The interchain exciton is usually called as a CT state, which can be described as a bounded electron-hole pair, where the hole and the electron are located on different molecules. Excitons can be either mobile or localized on an energy level below the edge of the conduction band.

The description of photogeneration of free charge carriers has been treated by many models. These models differ in the way how the bound pair of the

hole and the electron is formed and in the way how these pairs dissociate. The problem concerning the formation of bounded charge couples has not been fully solved yet. Bounded charge pairs can be formed either by direct photoexcitation or indirectly. Direct transitions are observed on molecular crystals unlike the polymers where only a indirect absorbtion is observed. Indirect formation of CT states starts with photoexcitation of the molecule to a higher singlet state followed by one of the following transitions:
a) autoionization of the excited state and thermalization of the localized hole and of the hot electron leading to an electrostatically bound pair
b) electron jumps to a neighboring molecule after the relaxation into the first excited singlet state
c) transformation of excitation energy from a donor to an acceptor and creation of the CT complex in the donor-acceptor pair.

The efficiency of the photogeneration of free charge carriers is described by a product of CT state creation probability and CT state dissociation probability. The efficiency of the CT state creation is described by a primary quantum yield and is denoted by η_0. The primary quantum yield describes probability of the CT state creation after absorption of one photon. This process is usually considered as independent of temperature and external electric field and dependent only on the energy of a photon. However, generally this process can depend on external electric field and phonons. The primary quantum yield is also affected by competing transitions in the molecule. Usually, before the creation of the CT state, the exciton undergoes migration, which can be up to tens nanometers in length. Such a distance is usually much smaller than the penetration depth of the absorbed light in organic compounds. This lowers the efficiency of organic solar cells and introduces a necessity of creating special nanostructures to increase the efficiency of photogeneration of free charge carriers.

Two basic theoretical models of the CT state dissociation can be found in the literature. The first one is a so-called Poole-Frenkel model. It is based on lowering Coulomb barrier between the hole and the electron in an external electric field. This model does not take into consideration a diffusion process. The second model is more sophisticated and takes into consideration drift and diffusive motion of the charge carrier in the internal and external electric field. This approach can be found in both the Onsager and Noolandi-Hong theories.

In the following subsections we will present some older models of photogeneration. A more complete description of these models can be found in [4].

2.1.1 Ballistic model

The ballistic model was developed by Silinsh[4, 5]. It was first used to describe photogeneration of free charge carriers in molecular crystals. This model considers photogeneration of free charge carriers as a process consisting of several steps. First step is a photoexcitation of the molecule followed by autoionization of the excited state. This results in a localized hole and a hot quasi-free electron, but depending on the organic material the electron can be localized and the hole can be mobile. Thermalization of the hot particle ends with the bounded electron-hole pair in which the electron and the hole are separated by a distance r_0. This model assumes that the dependence of the thermalization distance r_0 between charges is proportional to the square root of the surplus energy of the electron E_k. The energy E_k increases with the energy of the absorbed photon. These two physical quantities can be expressed as

$$r_0 = \sqrt{D\tau_{th}} = \sqrt{\frac{DE_k}{h\nu_{ph}^2}} \tag{2.1}$$

where τ_{th} is the thermalization time, D is the diffusion coefficient, ν_{ph} is the phonon frequency and h is the Planck constant. The autoionization yield is given by

$$\eta_0(h\nu) = \frac{k_{AI}(h\nu)}{k_{AI}(h\nu) + \sum_i k_i(h\nu)} \tag{2.2}$$

where k_{AI} and k_i are the rate constants of autoionization and intramolecular loss channels. It is assumed that η_0 can be larger for higher excited states. The primary quantum yield η_0 can generally depend on the absorbed photon energy.

The hot electron is assumed to be a Brownian particle with excess kinetic energy. This energy is dissipated by non-elastic scattering and acts against the Coulomb interaction between the hole and the hot electron. Due to the diffusive motion of the electron the thermalization distance r_0 is subjected to

a dispersion. The distribution of the thermalization distance can be described by the Gaussian distribution as follows

$$p(r) = \frac{1}{4\pi^{\frac{3}{2}} r_0^2 \sigma} \exp\left(-\frac{(r-r_0)^2}{\sigma^2}\right) \tag{2.3}$$

where σ is a parameter describing dispersion. The thermalization distance in solids is not higher than $10-15$ nm and $\sigma^2 \ll \langle r_0 \rangle^2$. For this situation Gaussian distribution function can be approximated by properly normalized δ function

$$p(r) = \frac{\delta(r-r_0)}{4\pi r_0^2} \tag{2.4}$$

with only one parameter.

2.1.2 Onsager model

The Onsager model is popular and widely used for interpretation of photogeneration in polymers and molecular crystals [4]. The creation of the electron-hole pair is described in the same way as in the ballistic model, i.e. as an indirect process. The difference between these two models arises in the modeling of the dissociation of the hole-electron pair with initial separation distance r_0. This problem is treated within the Onsager diffusion theory.

In this model the primary quantum yield η_0 is assumed to be independent on temperature T and external electric field F; all these dependencies are included in the dissociation step. The quantum yield of photogeneration of free charge carriers can be described as

$$\eta(F) = \eta_0 \int_{-\pi/2}^{\pi/2} \int_0^{2\pi} \int_0^{\infty} g(r,\theta) f(F,r,\theta) r^2 \sin(\theta) d\theta d\phi dr \tag{2.5}$$

where $g(r,\theta)$ is the initial space distribution of thermalized charge pairs, r is the distance between the hole and the electron, θ is the angle between the direction of the external electric field and the vector connecting the hole and the electron. The function $f(F,r,\theta)$ describes the probability that the hole-electron pair does not recombine. The function $f(F,r,\theta)$ fulfills the following boundary conditions $f(F,0,\theta) = 0$ and $f(F,\infty,\theta) = 1$. The dissociation of

the bound pair is described as Brownian motion of a particle in the Coulomb field of electron-hole pair and the external electric field F. The electric potential energy U can be written as

$$U = -eFr\cos\theta - \frac{e^2}{4\pi\epsilon_0\epsilon_r r} \tag{2.6}$$

where $F\cos\theta$ is the projection of the external electric field into the direction of the vector connecting the electron-hole pair, ϵ_0 is the permittivity of the vacuum, ϵ_r is the relative permittivity of the material, e is the elementary charge and r is the distance between the hole and electron. The function $f(F, r, \theta)$ can be calculated from the time independent Smoluchowski diffusion equation

$$\mathrm{div}(\exp(-U/(kT)\nabla f)) = 0. \tag{2.7}$$

The distribution of thermalized pairs $g(r, \theta)$ is described by δ function in solids and by Gaussian and exponential distribution functions in liquids. Separation distances obtained in this model by fitting experimental data are between $2 - 3$ nm [4]. Such high separation distances are hard to explain theoretically.

2.1.3 Knights-Davis model

This model, similarly as the first one, considers indirect creation of the bound pair [6]. It was developed to describe experimental results of photogeneration of free charge carriers in amorphous selenium. In this model we consider photogeneration of free charge carriers as a two-step process. The first step is the absorption of a photon followed by a thermalization leading to electron-hole bound pair. The thermalization of the electron-hole pair is accompanied by diffusion of the electron similarly as in the ballistic model. The second part of the photogeneration of free charge carriers is described by Poole-Frenkel mechanism as a dissociation of the bound pair facilitated by an external electric field. Quantum yield of the photogeneration of free charge carriers is determined by the ratio of the recombination time τ_r and ionization time τ_i as

$$\eta = \frac{1}{1 + \tau_r\tau_i^{-1}}. \tag{2.8}$$

Ionization time can be calculated in the following way

$$\tau_i = \nu_e^{-1} \exp \frac{\frac{e^2}{4\pi\epsilon r_0} + eFr_0 - \sqrt{\frac{e^3 F}{\pi\epsilon}}}{kT} \tag{2.9}$$

where ν_e is the frequency factor and ϵ is the permittivity of the material.

2.1.4 Noolandi-Hong model

This model was developed for the description of the photogeneration of free charge carriers in phthalocyanine thin films [7]. Experimental data on phthalocyanine showed the quantum yield independent on the excitation energy. This is explained in the following way; in the first step the molecule, excited by absorption of a photon to the higher excited state, looses surplus energy by fast internal conversion and the molecule stays in the first excited state with a relatively long lifetime. In the second step the excited state can either relax to the ground state or it can be autoionized forming a bound charge pair. The hole and the electron in the bound pair are located at different neighboring molecules. The probability of creation of the bound pair can be written as

$$k(\theta) = k_0 \exp(F F_0^{-1} \cos(\theta)) \tag{2.10}$$

where k_0, F_0 are constants and θ is the angle between the vector of the external electric field F and the vector connecting the electron and the hole. The probability of dissociation of the bound pair is obtained similarly as in the Onsager model. This probability can be obtained as a solution of the time-independent Smoluchowski equation (2.7). The boundary conditions in this model are different from those in the Onsager model. The Noolandi-Hong model considers also a recombination of bound pairs on a sphere of diameter r_m with finite recombination rate K, where r_m is a mean lowest intramolecular distance. The independence of the quantum yield on the energy of absorbed photons is caused by the losses of the surplus energy of the bound pair. The losses of the energy are caused by the internal conversion in the material.

Quantum yield for this model can be expressed as

$$\eta(F) = \frac{\overline{k(F)}}{\overline{k(F)} + k_n + k_r} \tag{2.11}$$

where k_r and k_n are rate constants of the radiative and non-radiative transitions of the excited state to the ground state and $\overline{k(F)}$ is

$$\overline{k(F)} = \frac{1}{2}\int_{-1}^{1} k(\cos\theta)\Omega(F, r, \cos(\theta))d(\cos\theta) \tag{2.12}$$

where Ω is the dissociation probability of bound pair separated by a distance r. This model has three tunable parameters: F_0, $\frac{k_n+k_r}{k_0}$ and $\frac{K}{D}$. One special limit of these parameters gives us the Onsager model.

2.2 Arkhipov model

In this section we present the Arkhipov model described in [1]. This model was designed to explain the photogeneration of free charge carriers in conjugated polymers doped by either electron donors or acceptors. Similarly as other models it consists of two steps. In the first step an exciton transforms into a coulombically bound pair. This step is realized in the place of a charge transfer, which is usually localized on the site of a dopant or alternatively in the neighborhood of a deep potential well. In the second step the bound pair dissociates into free charge carriers in an applied external electric field. The description of temperature and electric field dependencies of exciton transformation into Coulomb bound pair is not fully explored within this model.

It is assumed that after the absorption of a photon the created exciton travels along the polymer backbone. It moves through several conjugated segments before it either relaxes into the ground state or transforms into the bound state in the place of charge transfer. The probability of the exciton dissociation w_d can be calculated from the relative rate of exciton relaxation without dopants and from the probability of the tunneling of the electron to the electron acceptor in the distance d from the main polymer backbone. These processes can be described using the mean exciton lifetime τ and the tunneling rate $\nu_0 \exp(-2\gamma d)$, where ν_0 is the frequency factor and γ is the inverse localization length. Putting it together we obtain the total probability of the exciton dissociation in the following form

$$w_d = \frac{1}{1 + \frac{\exp(2\gamma d)}{\nu_0 \tau}} \tag{2.13}$$

It can be easily seen that the exciton dissociation rate decays exponentially with growing d.

After the exciton dissociation the electron is localized in a distance d from the polymer backbone. The hole remaining on the polymer backbone is trapped in a potential well $U(r)$, which is obtained as a sum of the external electric field F and Coulomb electric field of the localized electron. $U(r)$ can be written in the following form

$$U(r) = -eFzr - \frac{e^2}{4\pi\epsilon_0\epsilon_r\sqrt{(r^2+d^2)}} \tag{2.14}$$

where $z = \cos(\theta)$, θ is an angle between the direction of the external electric field and the polymer backbone, r is the distance measured along the polymer backbone and F is the absolute value of the external electric field. For sufficiently large F or d the function $U(r)$ monotonously decreases with respect to r. When such situation occurs, the charge carriers become free immediately after the exciton dissociation. If this is not the case the function $U(r)$ has a local minimum for certain distance $r = r_{min}$ around which the hole is trapped. We assume that the hole can escape the potential well by thermal activation. In order to calculate the escape probability of the hole, we need to calculate the potential barrier. This is done by approximating the potential well as a harmonic potential. By the help of the Taylor expansion to the second order we rewrite $U(r)$ around r_{min} and we obtain the potential $U_{osc}(r)$ in the form

$$U_{osc}(r) = -eFzr_{min} - \frac{e^2}{4\pi\epsilon_0\epsilon_r\sqrt{r_{min}^2+d^2}} + \frac{e^2(d^2-2r_{min}^2)}{8\pi\epsilon_0\epsilon_r(r_{min}^2+d^2)^{\frac{5}{2}}}(r-r_{min})^2 \tag{2.15}$$

The last part of the previous equation describes the energy of the oscillating hole within the potential well. The minimal energy of the charge carrier E_{min} can be calculated as a sum of the minimum of the potential $U_{osc}(r)$ and the energy of zero point oscillation. We obtain the following

$$\begin{aligned} E_{min} = U_{osc}(r_{min}) + \frac{1}{2}\hbar\omega = -eFzr_{min} - \frac{e^2}{4\pi\epsilon_0\epsilon_r(r_{min}^2+d^2)^{\frac{1}{2}}} \\ +\hbar\sqrt{\frac{e^2(d^2-2r_{min}^2)}{16\pi\epsilon_0\epsilon_r(r_{min}^2+d^2)^{\frac{5}{2}}m_{eff}}} \end{aligned} \tag{2.16}$$

where $\hbar$ is reduced Planck constant, ω is the oscillation frequency and m_{eff} is the effective mass of the charge carrier. The equation (2.16) assumes an infinitely long polymer chain. In a real system the hole can move freely only within a conjugated segment. This narrows the potential well and affects oscillation energy of the hole.

The height of the potential barrier needed to be overcome by the hole can be calculated as a difference between the local maximum of the potential $U_{max} = U(r_{max})$ and the minimal energy E_{min}. There are two limiting cases when the dissociation of the bounded state happens immediately after the exciton dissociation. One of them was already discussed above, it is when the potential $U(r)$ is monotonous with respect to r. Another one is when there is a potential well, but it is so shallow that the harmonic approximation done in (2.15) is unacceptable and, therefore, the minimal energy of the hole would be formally greater than the local maximum of the potential $E_{min} > U_{max}$. It can be shown by direct calculation that the height of the potential well increases with decreasing d. Because the potential barrier depends on z we can find such a function $d_0(z)$ for which $E_{min}(d_0, z) = U_{max}(d_0, z)$ is satisfied. It means that we can find a critical initial separation distance depending on z for fixed F. For values d greater then this critical value, i.e. for such d which fulfills

$$d > d_0(z), \tag{2.17}$$

the dissociation of CT state occurs immediately after the exciton dissociation. This is in reality not very probable because with increasing d the probability of CT state creation decreases exponentially. When the condition (2.17) is not fulfilled additional thermal activation is needed to create free charge carriers. The hole has to escape from the potential well before recombination with the trapped electron. We denote the rate of the hole recombination as ν_{rec}. The recombination rate is governed by the tunneling rate of the electron and it can be written as

$$\nu_{rec} = \nu_0 \exp(-2\gamma d) \tag{2.18}$$

The escape of the hole from the potential well is a thermally activated process and its rate can be written as

$$\nu_{esc} = \nu_0 \exp\left(\frac{E_{min}(d) - U_{max}(d)}{kT}\right) \tag{2.19}$$

Now, if we combine equations (2.13) and (2.18) we obtain the total probability of creation of free charge carrier from one photon absorption $w = w(d, z)$ depending on d and z as

$$w = [1 + (\nu_0\tau)^{-1}\exp(2\gamma d)]^{-1}\left\{1 + \exp[-2\gamma r + \frac{U_{max}(d,z) - E_{min}(d,z)}{kT}]\right\}^{-1} \tag{2.20}$$

the expression (2.20) describes photogeneration of free charge carriers for fixed d and θ. In a real polymer material molecules are randomly oriented as well as electron acceptors are randomly distributed. If we are interested in the quantum yield of the photogeneration of free charge carriers in such materials we have to average the probability w with respect to the distribution of the distance d of the traps from the polymer chain and also with respect to the random orientation of the polymer chain with respect to the direction of the applied electric field. We assume that distribution of electron acceptors $P(d)$ in a polymer material can be approximated by the Poisson distribution which can be written as

$$P(d) = 2\pi r l N_d \exp[-\pi l N_d (d^2 - d_{min}^2)] \tag{2.21}$$

where l is the length of a conjugated segment, d_{min} is minimal distance of the electron acceptors from the polymer backbone and N_d is the concentration of electron acceptors . The quantum yield η of photogeneration of free charge carriers can be written as

$$\begin{aligned}\eta = \frac{2\pi}{N_d}\int_0^1 dz \int_{\max\{d_{min},d_0(z)\}}^{\infty} dx \quad & \frac{x\exp[\frac{-\pi}{N_d}(x^2 - d_{min}^2)]}{1 + (\nu_0\tau)^{-1}\exp(2\gamma x)} + \\ + \int_0^1 dz \int_{d_{min}}^{\max\{d_{min},d_0(z)\}} dx \quad & \frac{x\exp[\frac{-\pi}{N_d}(x^2 - d_{min}^2)]}{1 + (\nu_0\tau)^{-1}\exp(2\gamma x)} \cdot \\ \cdot \left\{1 + \exp\left[-2\gamma x + \frac{U_{max}(d,z) - E_{min}(d,z)}{kT}\right]\right\}^{-1} & .\end{aligned} \tag{2.22}$$

where we averaged the probability w over the distribution $P(d)$ over the random orientation of the polymer chains.

2.3 Modified Arkhipov model

A modification of the original model of Arkhipov [1] was done in [2]. The difference between the original model and the modified one is the following; there is a possibility that the charges in CT state can recombinate back forming an exciton. This enables additional cycling in the model. Another difference of this model to the original one is that it deals with a pure polymer, containing neither donors nor acceptors. Instead of an additive, another molecule of the polymer serves as the acceptor of the electron in the photogeneration process.

In this model, similarly as in the original one, we assume that after absorption of a photon the created exciton travels along the π-conjugated system. It can be transformed into a CT state with a probability η_0. The transformation of the exciton into a CT state can occur at points where two polymer chains come close to each other. The transformation of the exciton into the CT state proceeds via an intermolecular jump of the electron. After the jump the hole and the electron could theoretically move independently in an external electric field as long as the Coulomb interaction between them is overcome. In conjugated systems the mobility of the hole μ_d is higher than the mobility of the electron μ_e and, as a result, holes are the dominant free charge carriers formed after the dissociation process. In this model the hole escapes from the potential well formed around the electron, which is less mobile than the hole. In this aspect it is very similar to the Arkhipov model [1].

The hole is influenced by the potential described in the same way as in the original Arkhipov model, i.e. a sum of potentials of the external electric field and of the Coulomb interaction between the hole and the electron. This potential $U(r)$ can be written as in (2.14) where we denote d as a separation distance between the neighboring chains and r as the distance traveled by the hole along the chain away from the localized electron. As a simplification we assume that ϵ_r is independent on r. Because we are working with the same potential as in the previous case its properties remain unchanged. We denote the coordinate for which the minimum of the potential $U(r)$ is achieved as r_{min}. The procedure how to calculate the value of r_{min} are presented in [1]. The conditions under which this local minimum can be calculated are described in [2]. The escape of the mobile hole trapped in the potential

well of $U(r)$ is a thermally activated process with a rate constant k_{esc}. This constant can be calculated in a similar manner as before

$$k_{esc} = k_0 \exp\left\{\frac{-(U(r_{esc}) - E_{min})}{kT}\right\} \tag{2.23}$$

where k_0 is a constant. There are two versions of this model depending on whether we allow the resonant coupling of the exciton state and the CT state or not.

2.3.1 "One-step" model of exciton dissociation and recombination of CT state

This model coincides with the original Arkhipov model. We assume that the CT state can either dissociate into free charge carriers or recombinate into the ground state and we neglect the possibility of the CT state transformation back into the exciton. We denote the rate constant of the recombination as k_{rec}. The probability of the CT state dissociation p_{esc} can be written as

$$p_{esc} = \frac{k_{esc}}{k_{esc} + k_{rec}} = \frac{1}{1 + \frac{k_{rec}}{k_0} \exp\{\frac{U(r_{esc}) - E_{min}}{kT}\}}. \tag{2.24}$$

The ratio

$$A = \frac{k_{rec}}{k_0} \tag{2.25}$$

can be interpreted as a one-step relative recombination constant. Quantum yield of the photogeneration of free charge carriers can be written as a product of the probability of the CT state creation represented by the primary quantum yield and the probability of the CT state dissociation into free charge carriers. This can be expressed as

$$\eta = \eta_0 p_{esc} \tag{2.26}$$

where η_0 denotes the primary quantum yield.

2.3.2 Model with resonant coupling of exciton and CT state

In this subsection we discuss the situation when the exciton and the CT state are energetically close to each other or even at a resonance, which

results in an exciton localization by a self-trapping. Such coupling of the CT state and the exciton leads to multiple transitions between the exciton and the CT state. When such situation occurs, it is impossible to introduce the primary quantum yield as in the previous case and we have to consider effects resulting from "cycling". In order to do so properly, we need to describe elementary processes in our model and then we have to solve the kinetic equations describing the system. The processes considered after the initial creation of the exciton by photoexcitation in our model are the following:
a) the exciton can either transform into the CT state with a rate constant k_1 or relax into the ground state with a rate constant k_g^{EX}.
b) the CT state can either dissociate into free charge carriers with a rate constant k_{esc} or relax into the ground state with rate constant k_g^{CT} or it can be transformed back into the exciton with a rate constant k_{-1}.
All the listed processes are summarized in Figure 2.1.

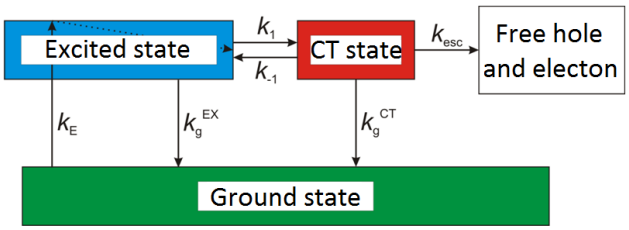

Figure 2.1: Processes of the photogeneration of free charge carriers with included resonant coupling with their respective rate constants; CT state and exciton coupling (k_1, k_{-1}), loss channels (k_g^{EX}, k_g^{CT}), photogeneration of exited state (k_E) a creation of free charge carriers (k_{esc}).

The quantum yield of the photogeneration of free charge carriers η can be expressed as the ratio of the concentration of the created free charge carriers and the absorbed photons per unit volume.

$$\eta = \frac{k_{esc}[CT]}{\Phi_{abs}} \tag{2.27}$$

where Φ_{abs} denotes the rate of photon absorption per unit volume and $[CT]$ is the concentration of CT states. If we want to calculate the concentration of CT states we need to solve a set of kinetic equations describing the processes

in Figure 2.1. These equations can be written as

$$\begin{aligned} \frac{d}{dt}[EX] &= f\Phi_{abs} - k_1[EX] - k_g^{EX}[EX] + k_{-1}[CT] \\ \frac{d}{dt}[CT] &= k_1[EX] - k_{esc}[CT] - k_{-1}[CT] - k_g^{CT}[CT], \end{aligned} \tag{2.28}$$

where f is a rate constant describing the initial singlet state transformation S_1 into exciton and $[EX]$ is the concentration of the excited states. One of the possible ways how to solve equations (2.28) is to use the steady state assumption, i.e. $\frac{d}{dt}[EX] = 0$ and $\frac{d}{dt}[CT] = 0$. A straightforward results in

$$\eta = \frac{k_1}{k_1 + k_g^{EX}} f \frac{k_{esc}}{k_{esc} + k_{-1} + k_g^{CT} - \frac{k_{-1}k_1}{k_1 + k_g^{EX}}}. \tag{2.29}$$

We can rewrite the previous equation as

$$\eta = \eta_{eff} \frac{k_{esc}}{k_{esc} + k_{rec}^{eff}}, \tag{2.30}$$

where η_{eff} is the effective primary quantum yield of charge carrier photogeneration

$$\eta_{eff} = \frac{k_1}{k_1 + k_g^{EX}} f_0 \tag{2.31}$$

and k_{rec}^{eff} is the effective rate constant of CT state recombination

$$k_{rec}^{eff} = k_{-1} + k_g^{CT} - \frac{k_{-1}k_1}{k_1 + k_g^{EX}} = k_g^{CT} + \frac{k_{-1}k_g^{EX}}{k_1 + k_g^{EX}}. \tag{2.32}$$

Formally the equation (2.30), derived to the modified Arkhipov model, and (2.24) belonging to the original Arkhipov model look to be the same, but they differ in the possible dependence of parameters η_0^{eff} a k_{rec}^{eff}. Contrary to the original model, the modified model parameters are allowed to depend on the external electric field. It effects the fact that external electric field affects energy difference between CT states and, hence, it influences the detailed balance conditions between the occupation of the excited states and CT states. Consequently, the rate constants k_1 and k_{-1} become dependent on the external electric field and, in the same way, also the rates η_0^{eff} a k_{rec}^{eff}

become dependent on the external electric field. The total quantum yield within the modified Arkhipov model can be written as

$$\eta = \eta_{eff} \frac{1}{1 + A_{eff} \exp(\frac{U(r_{esc}) - E_{min}}{kT})} \tag{2.33}$$

where $A_eff = \frac{k_{rec}^{eff}}{k_0^{eff}}$ is effective preexponential factor.

2.4 Quantum-chemical calculations

In this section we briefly mention essentials of the ab initio quantum calculations. The task to be solved is to find eigenvectors and eigenvalues of the Hamiltonian in the following form

$$\begin{aligned} H = &- \sum_{j \in N} \frac{\hbar^2}{2M_j} \Delta_{N,j} - \sum_{j \in M} \frac{\hbar^2}{2m_e} \Delta_j + \sum_{j \in N} \sum_{k \in N} \frac{e^2 Z_j Z_k}{4\pi\epsilon_0 |Q_j - Q_k|} \\ &- \sum_{j \in N} \sum_{k \in M} \frac{e^2 Z_j}{4\pi\epsilon_0 |Q_j - q_k|} + \sum_{j \in M} \sum_{k \in M} \frac{e^2}{4\pi\epsilon_0 |q_j - q_k|} \end{aligned} \tag{2.34}$$

where N and M denotes the number of atoms and electrons in the system respectively, M_j is the mass of the j-th atom nucleus, m_e is the mass of the electron, Z_j is the charge of the j-th atom nucleus, $-\Delta_{N,j}$ and $-\Delta_j$ denotes the Laplace operator of j-th atom and j-th electron respectively, Q_j and q_k are the positions of the j-th atom and k-th electron respectively and lastly $\hbar$ is reduced Planck constant. By neglecting the relativistic effects we employed the first simplification. These effects can be added by the means of the perturbation theory or with help of relativistic pseudopotentials [8]. Such system with the Hamiltonian H is not solvable analytically for the case that $N + M > 2$. For this reason we have to employ certain simplifications. The most important is a Born-Oppenheimer approximation, based on the separation of electrons and atom nuclei. The motion of the nuclei can be then solved either classically or by quantum mechanical calculations. There are many ways how one can address the problem of the electrons. We will briefly describe two methods, which we use in our work.

2.4.1 Hartree-Fock method

First method, we describe, is so called Hartree-Fock method (HF). We need to solve the equation

$$H_{el}\psi = E\psi \tag{2.35}$$

where the operator H_{el} can be written as

$$\begin{aligned} H_{el} = &- \sum_{j\in N} \frac{\hbar^2}{2M_j}\Delta_{N,j} - \sum_{j\in M} \frac{\hbar^2}{2m_e}\Delta_j \\ &- \sum_{j\in N}\sum_{k\in M} \frac{e^2 Z_j}{4\pi\epsilon_0|Q_j - q_k|} + \sum_{j\in M}\sum_{k\in M} \frac{e^2}{4\pi\epsilon_0|q_j - q_k|} \end{aligned} \tag{2.36}$$

This equation can be solved exactly for $N \leq 2$. For more than two electrons we have to employ certain approximations. The HF method is a variational method using the approximation of independent electrons [8]. In this method we are searching for the solution of the associated variational problem in the form of a single Slater determinant. The model of independent electrons assumes that the electron moves in the mean electric field generated by all the other electrons in the system. This leads to the self consisting field problem which is solved iteratively. The main problem of this approach is that we are not able to obtain electron correlation correctly. This error can be fixed by many post HF methods, for example by Møller-Plesset perturbation theory, where the correlations are added as a perturbation term. One of the important applications of the HF method is so called Koopman's Theorem. This theorem states that the ionization potential of a closed-shell molecule can be calculated as a minus energy of the highest occupied molecular orbital. This approach gives surprisingly good results which is caused by the compensation of the multiple errors. For more details we refer the reader to the monograph [8] or [9].

2.4.2 Density functional theory

Another approach we employ later is the density functional theory (DFT). This method is based on the Hohenberg-Kohn theorems [9]. These theorems state that for the electron system with the non-degenerate ground state without magnetic field the ground state eigenfunction can be expressed as the function of the total electron density. By this approach we are able to

solve the problem of the function depending on three spatial coordinates only and not on the $3N$ electron spatial coordinates. The energy of the system is then given by appropriate functional. The problematic part of this process is to find such functionals which would give us the appropriate solution. The most problematic task is to calculate the exchange correlation energy. There is a large variety of different functionals available, from those calculated theoretically to those, which are obtained by fitting the experimental data. For our purpose we chose hybrid functional B3LYP presented in [10, 11]. The hybrid functionals are special case of DFT method which treats the problem with the exchange correlation energy in such a way that the exchange correlation energy is calculated partially from the exact exchange correlation energy from HF method and partially from other sources. The DFT methods are often used for the calculation of oligomers [12, 13]. They are also used for the calculation of various σ-conjugated and π-conjugated systems [14, 15]. Calculations of ion-radical systems can be done within the DFT methods successfully [14, 15].

Chapter 3

Calculations of the polymer structure

In this chapter we present results of the quantum-chemical calculations of the configuration and of the conformation of the polymer on which the modeling of the charge carrier photogeneration will be performed. Finding the right structure of the polymer chain, mutual position of adjacent chain, as well as the charge distribution in the cation-radical and anion-radical, are essential for later calculations of the photogeneration process. Ab initio quantum-chemical calculations were done using Gaussian software [16]. Chains of the studied polymer were modeled as oligomers, each one consisted of 10 monomer units. Poly[1-(trimethylsilyl)phenyl,2-phenylacetylene] was the polymer under study in this work.

3.1 Geometry of a single polymer chain

The first thing we had to know about the polymer was the configuration of the polymer backbone. We studied theoretically three options how the monomer units can be connected. The studied options were: head-to-head, head-to-tail and tail-to-tail. In Figure 3.1 these configurations are denoted by the type of bonding of the first two monomer units. We considered only the regular configurations. We decided which configuration is the most stable one by comparing the ground state energies of the neutral molecules in its optimal geometries. The energy of those configurations were calculated in the following way. First, we calculated the optimal geometry for our decamers using

Head-to-head configuration
TH–HT–TH–HT–TH–HT–TH–HT–TH–HT

Head-to-tail configuration
TH–TH–TH–TH–TH–TH–TH–TH–TH–TH

Tail-to-tail configuration
HT–TH–HT–TH–HT–TH–HT–TH–HT–TH

Figure 3.1: Studied possibilities of bonding of monomer units.

the Hartree-Fock method in the basis of atomic orbitals 6-31G* [17, 18]. We took these structures as an initial guess of the geometry for the density functional theory calculation. As a density functional theory functional we chose a hybrid functional B3LYP [10]. In addition to the standard B3LYP functional we have considered also this functional supplemented by an empirical correction term [19] describing the dispersion interaction between the atoms in molecule. The reason for this approach is a relatively strong interaction coming from the Van der Waals forces between the adjacent phenyl groups. These interactions are not described well in the original B3LYP functional. The calculations without added dispersion are denoted by abbreviation DFT and the calculations with added dispersion by DFTD. Both calculations by DFT and DFTD method were done in the basis of atomic orbitals 6-31G*. The calculations have shown that the most stable configuration is the one with the head-to-tail arrangement. However, the difference between the energies of the ground states of these configurations is so small that all three configurations are possible and the final configuration of the polymer could be influenced by the method of the preparation. The ground state energy is summarized in Table 3.1.

Table 3.1: Ground state energy of decamer in Hartrees

Configuration	B3LYP	B3LYP+dispersion
Tail to tail	-9482.92165887	-9483.72267259
Head to tail	-9482.92251630	-9483.74275046
Head to head	-9482.92013676	-9483.72502132

Table 3.2 shows these energies listed in kJ per mole. For the conversion

we used units the conversion factor $1\,\text{Hartree} = 2625.4996\,\frac{\text{kJ}}{\text{mole}}$ [20].

Table 3.2: Ground state energy of decamer in kJ per mole

Configuration	B3LYP	B3LYP+dispersion
Tail to tail	-24897407	-24899510
Head to tail	-24897409	-24899563
Head to head	-24897403	-24899516

The difference between the energy of different configurations was bigger if DFTD method was used. The reason for this is that the dispersion is dependent on the mutual position of phenyl groups. Dispersion is also affected by position of trimethylsilyl groups with respect to each other. In the tail-to-tail configuration and in the head-to-head configuration the trimethylsilyl groups are not so close to each other than they are in the head-to-tail configuration. Experimental study of the configuration of our polymer was not done.

Configurations of all polymer chains look quite similar. The polymer backbone is twisted into helical structure and the side groups of the polymer (phenyl and 4-(trimethylsilyl)phenyl groups) are directed away from each other as much as they are allowed.

It is worth mentioning that for a polymer of infinite length the configuration head-to-head is the same as tail-to-tail. The difference between them arises from the different end groups, where for one configuration there are phenyl side groups and for another one 4-(trimethylsilyl)phenyl side groups.

Visualization of the optimal geometries of different configurations can be seen in Figures 3.2-3.4. Here we omitted hydrogens for better clarity of figures. Silicon atoms are denoted by pink color, carbon atoms of the main backbone are orange and carbon atoms of the sidegroups are grey.

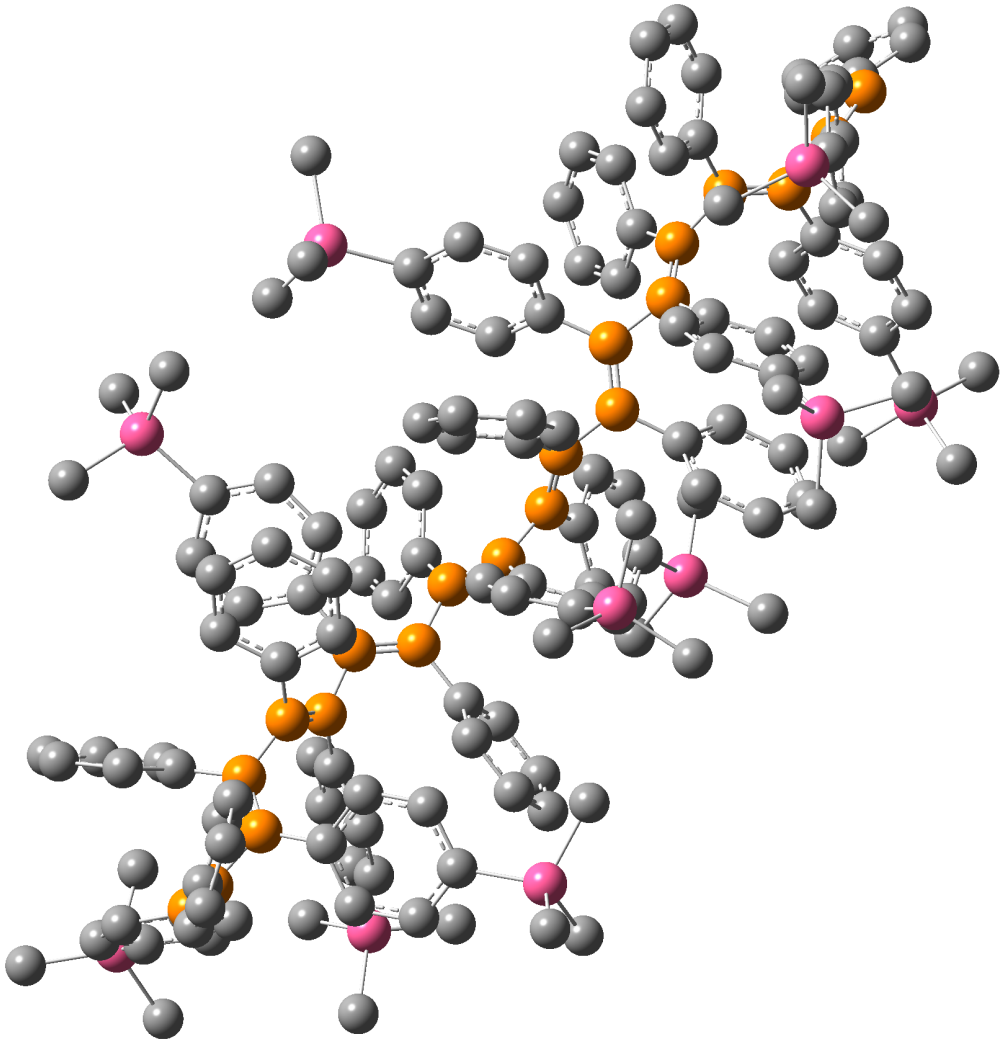

Figure 3.2: Optimal geometry of the decamer in the tail-to-tail configuration calculated by the DFTD method.

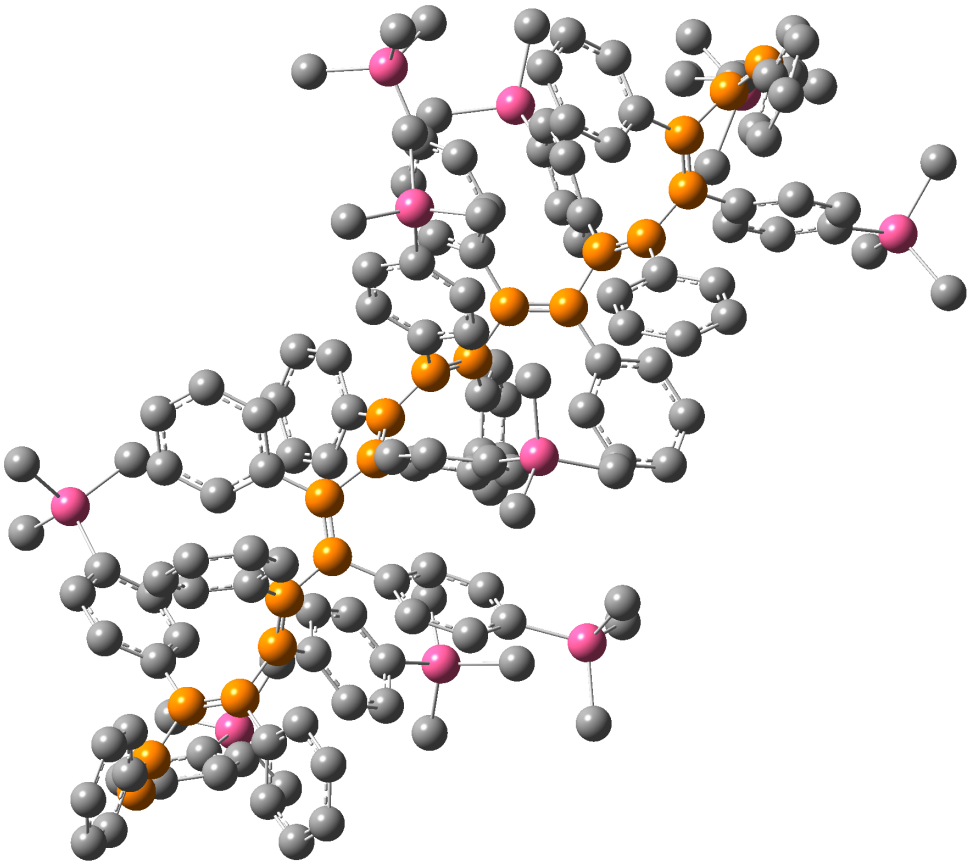

Figure 3.3: Optimal geometry of the decamer in head-to-tail configuration calculated by the DFTD method.

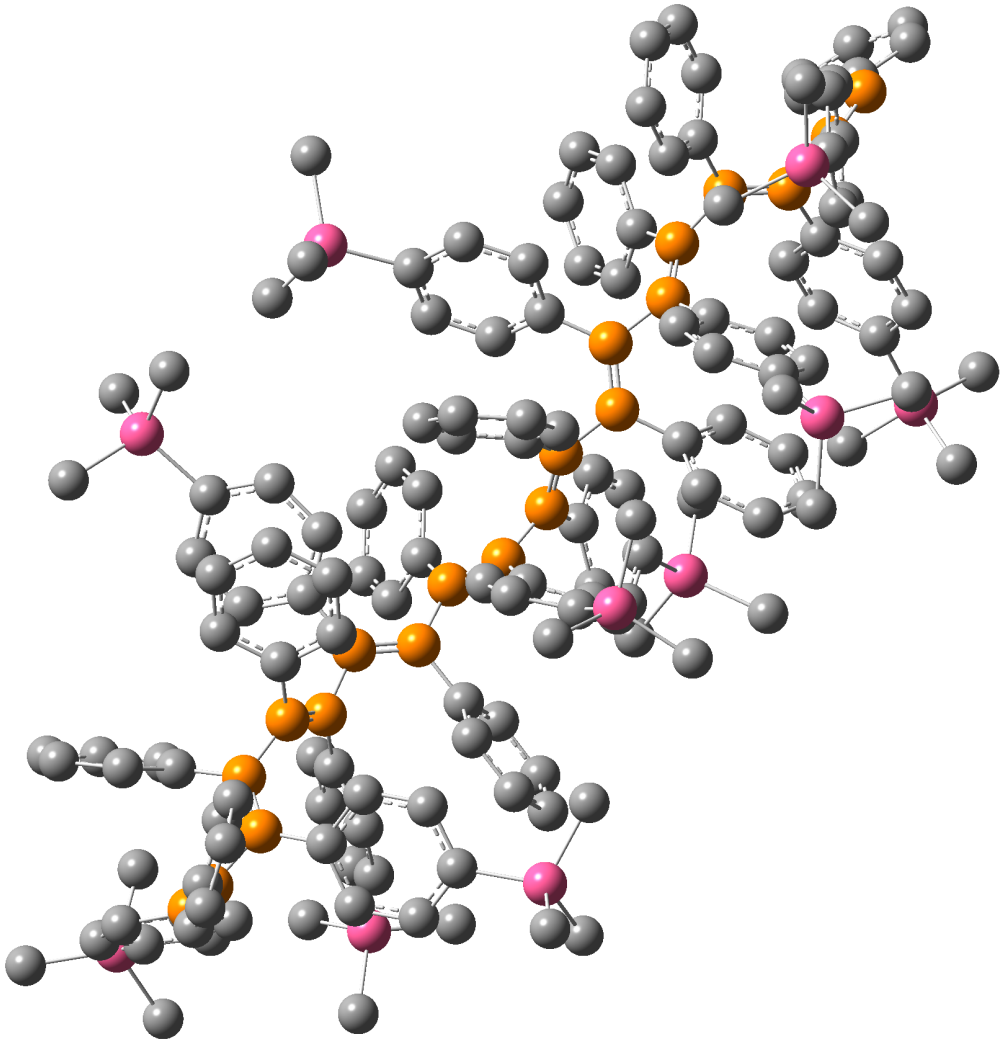

Figure 3.4: Optimal geometry of the decamer in head-to-head configuration calculated by the DFTD method.

In the following graphs we show some basic properties of the polymer chain. In Figure 3.5 we can see the length of the bonds of different decamer configurations calculated by DFT and DFTD method, especially we can see that the bond lengths are not dependent on the configuration of the decamer but only on the method which we chose. Calculation with added dispersion gives shorter bonds lengths. In these graphs we can see the alternation of the bonds of two lengths. The length around 152 pm corresponds to the single bond and the length around 136 pm corresponds to the double bond.

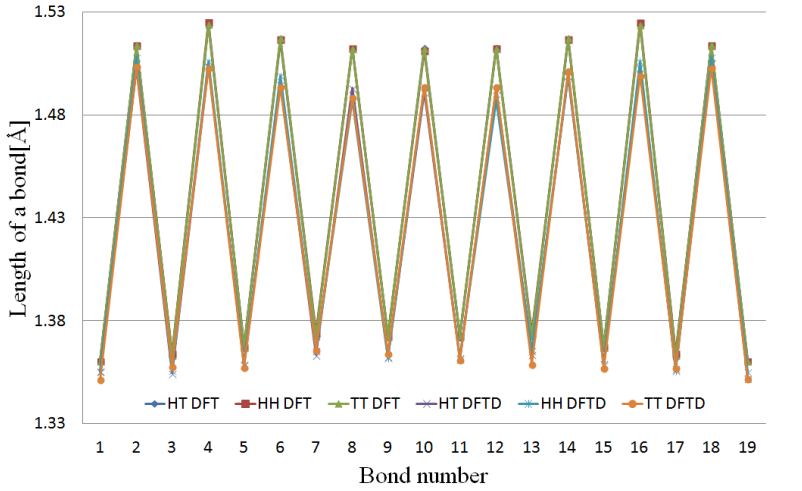

Figure 3.5: Bond lengths in the polymer backbone calculated by the DFT and the DFTD method.

In Figures 3.6 and 3.7 we show the bond angles along the polymer backbone calculated by DFT and DFTD method. We can see especially for the DFT method that in the middle of the chain we have a periodic structure, which is broken at both ends of the chain. This fact is nicely seen on the dihedral angles along the polymer backbone. However, we can see that the bond angle along the polymer backbone varies only slightly between the values 117-120 degrees.

In Figure 3.8 we have the dihedral angle along the polymer backbone. We can see that the dihedral angle changes quite significantly. We can see that the periodic structure, which can be seen in the middle, is broken at

Figure 3.6: Bond angles along the polymer backbone calculated by the DFT method.

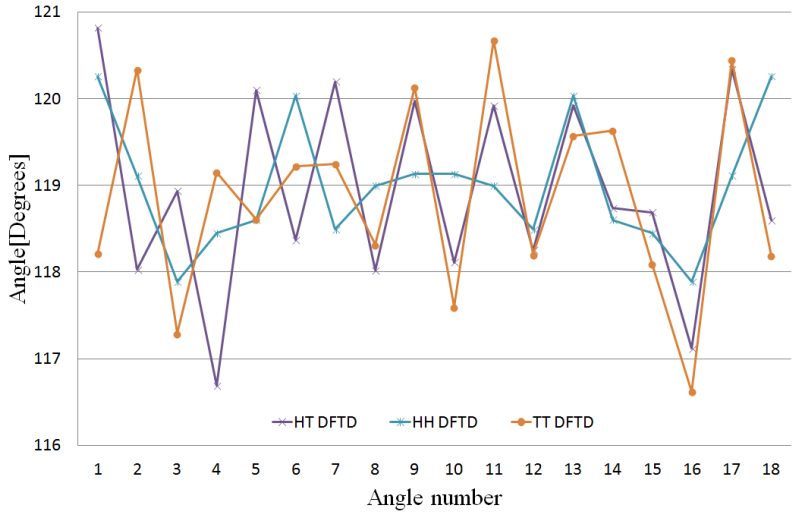

Figure 3.7: Bond angles along the polymer backbone calculated by the DFTD method.

the ends of the chain. Also the dihedral angle in the middle of the molecules has only two values, namely 130 degrees and 165 degrees, with the exception of geometry of the tail-to-tail configuration calculated by the DFTD method.

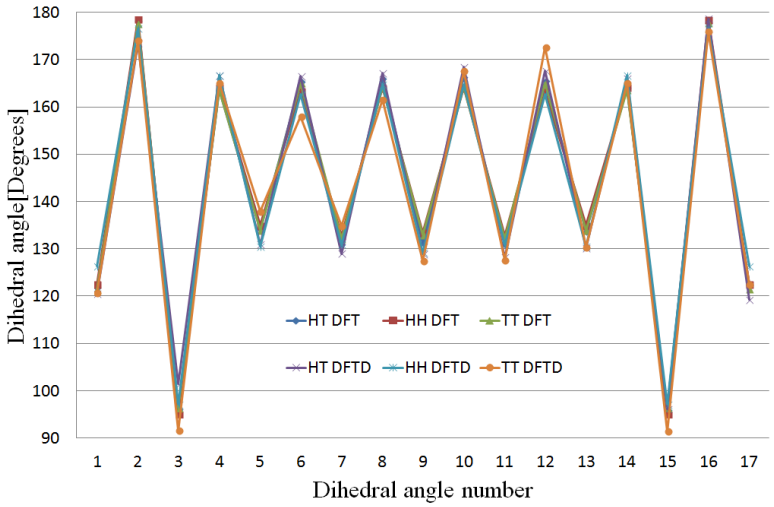

Figure 3.8: Dihedral angles along the polymer backbone calculated by the DFT and the DFTD methods.

From now on we will discuss only the head-to-tail configuration as the most stable configuration of the polymer. For the following calculations we also need to know the equilibrium geometries of the anion-radical and the cation-radical. These calculations were done by the DFTD method in the atomic basis 6-31G*. This basis lacks the diffuse functions which are often added during the calculations of ion-radicals. The large size of our system with respect to the available computation resources was our reason for omitting them.

We show the difference between the calculated geometry of the neutral molecule and of the ion-radicals in the following figures. If we compare the geometry of the neutral chain and with that of the anion-radical and the cation-radical, respectively, we find out that the geometry has been only slightly changed. The motif of the helix is preserved. The relevant variables for comparing the shape of the polymer backbone are summarized in Figures 3.9-3.11. There are only slight changes in bond angles and dihedral angles along the polymer backbone. The lengths of the bonds in the polymer backbone (see Figure 3.11) changes more significantly. The difference in the bond lengths is largest in the middle of the polymer backbone, which is the place

of the largest change in the spin density as we will show later.

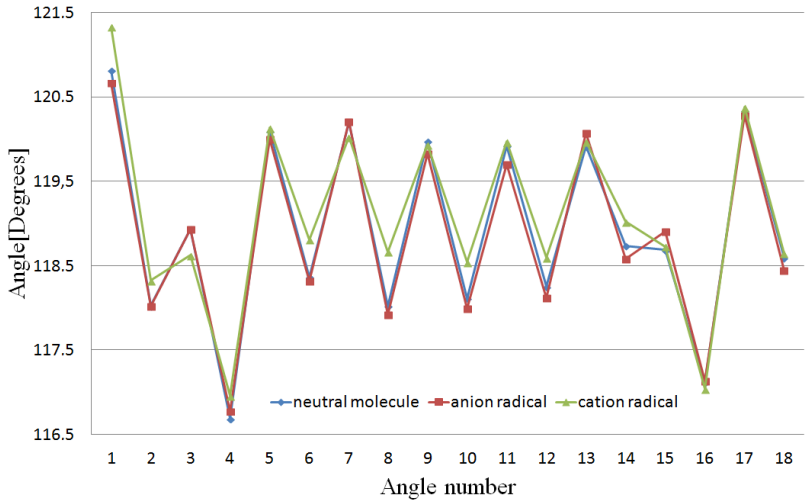

Figure 3.9: Bond angles along the polymer backbone calculated by the DFTD method for the head-to-tail configuration.

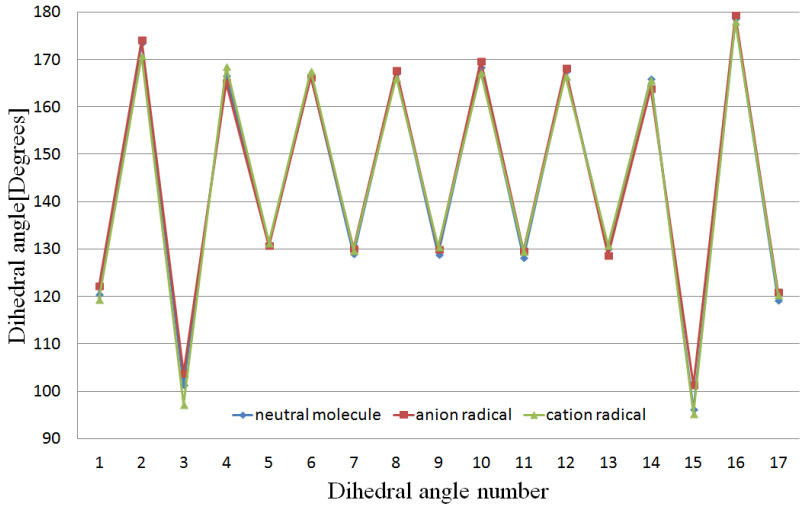

Figure 3.10: Dihedral angles along the polymer backbone calculated by the DFTD method for the head-to-tail configuration.

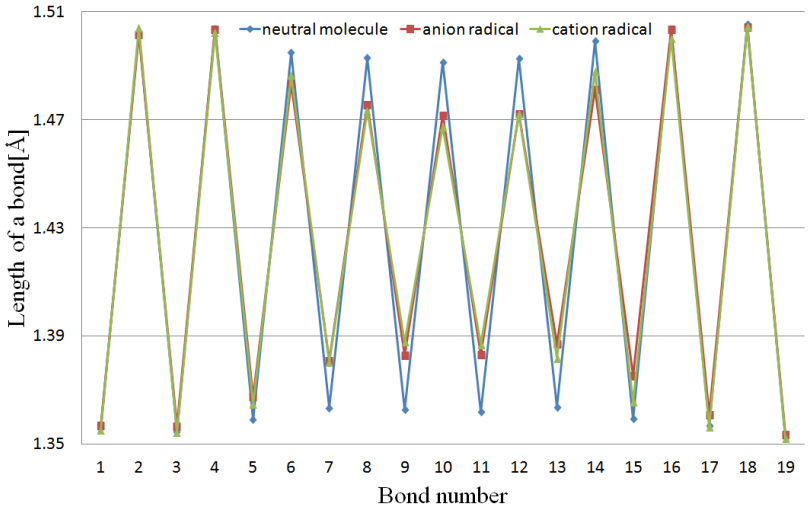

Figure 3.11: Bond lengths of the polymer backbone calculated by the DFTD method for the head-to-tail configuration.

In the modified Arkhipov model we expect that the charge transfer state can be represented as a hole located on the chain, which was excited by an absorbed photon, and an electron localized on one of the adjacent polymer chains. It was presumed that the electron is localized on the side group and the hole is trapped and delocalized on the main polymer backbone in a potential well caused by Coulomb interaction between the electron and the hole. We show that this notion is reasonable to certain degree.

In the following figures we present Mulliken spin and Mulliken charge densities. The purpose of this analysis was to estimate where the hole and the electron are localized on the cation-radical and on the anion-radical, respectively.

In Figure 3.12 we show Mulliken charge densities on the carbon atoms of the polymer backbone for the neutral molecule, the anion-radical and the cation-radical. These densities vary along the polymer chain only negligibly. From this picture one could wrongly assume that not the hole nor the electron are localized on the polymer backbone. We explain this discrepancy below.

In Figure 3.13 we have summed Mulliken charge distributions on the side groups along the polymer backbone. We can see that there is a large difference in these densities between the neutral molecule and ion-radicals. This approach can give us a rough estimate of the localization of the charges forming the electric field that affects dissociation of the CT state. This approach, however, does not give us a right interpretation where the hole is localized in the cation-radical. To answer this question we need to look at the Mulliken spin densities. The reason, why knowing only the charge densities are not sufficient, is that the charge densities are shifted by the interaction of the electron spins, in open shell system compared to the situation in the closed shell system. The interaction between the same spins is repulsive.

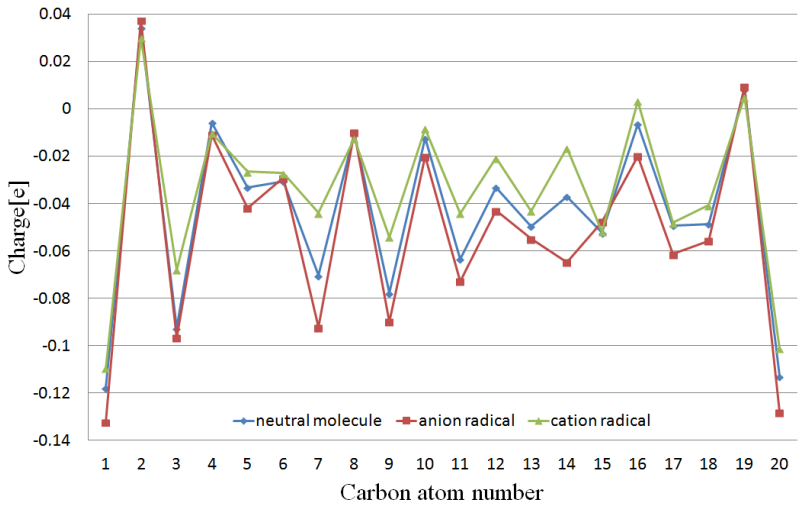

Figure 3.12: Mulliken charge distributions along the polymer backbone calculated by the DFTD method for the neutral molecule, anion radical and cation radical, respectively.

In Figure 3.14 Mulliken spin densities on carbon atoms of the polymer backbone for the neutral molecule, the anion-radical and the cation-radical are shown. We can see, in contrast to the Mulliken charge densities, that these densities vary along the chain significantly. If we simply summed the spin densities on the polymer backbone we would see that for the anion radical 65 percent of the spin density is localized on the polymer backbone and

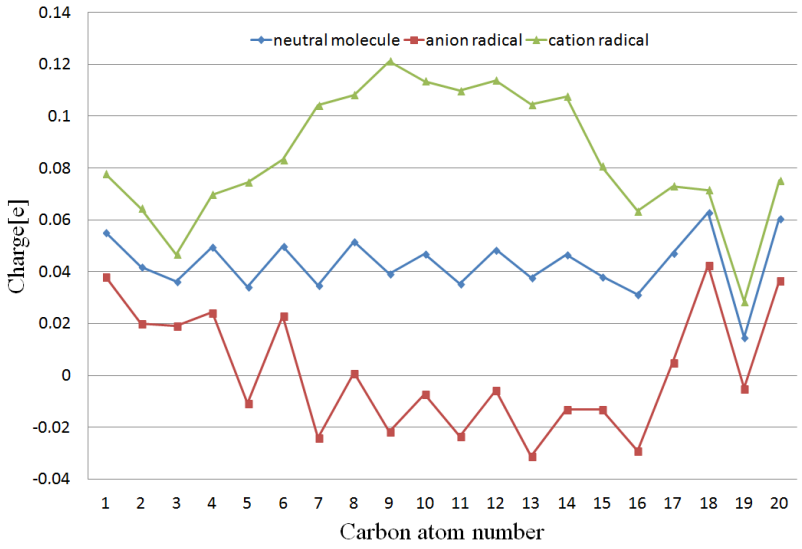

Figure 3.13: Summed Mulliken charge distributions on each side group along the polymer backbone calculated by the DFTD method for the neutral molecule, anion radical and cation radical, respectively.

for the cation-radical even 69 percent of the spin density occurs on the polymer backbone. In Figure 3.13 we have summed Mulliken spin distributions on each monomer unit along the polymer backbone. We can see that the spin densities are distributed for both the cation-radical and the anion-radical in a similar way. When we look at the spin densities summed on each monomer unit we see that the hole for the case of the cation-radical and the electron for the case of anion-radical are highly delocalized. If we considered longer chain in our calculation we would obtain even more extended delocalization.

It was interesting to see the oscillation of the spin density along the carbon atoms in the main backbone. We compared these results to the results of the spin density calculations on the acetylene-decamer to show that it is not the effect of sidegroups. We calculated these spin densities in anion-radical and cation-radical of the acetylene-decamer in two geometries:
a) ideal conjugation, i.e. planar model of the trans-oligoacetylene, and
b) in the geometry obtained for the main backbone of our decamer.
For the acetylene-decamer calculated with the geometry of the main backbone of our polymer we obtained essentially the same values as for our poly-

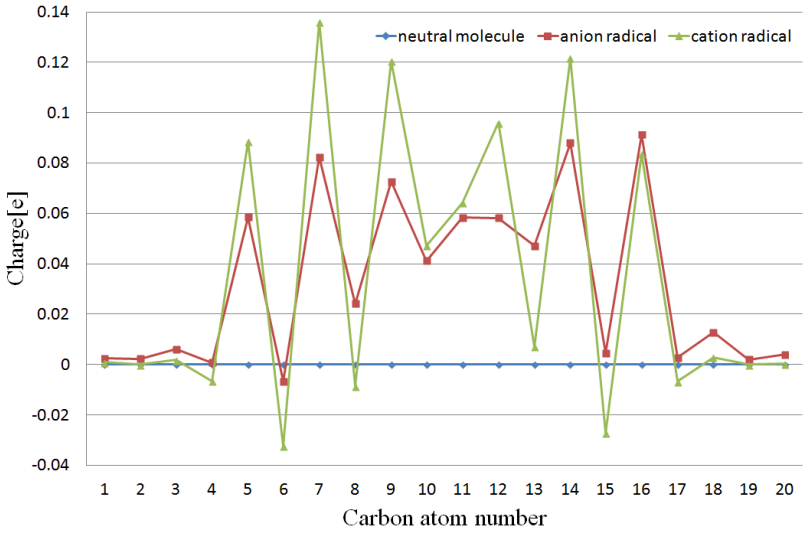

Figure 3.14: Mulliken spin distributions along the polymer backbone calculated by the DFTD method for the neutral molecule, anion radical and cation radical, respectively.

mer. For the planar model we obtained Mulliken spin densities presented in Figure 3.16. These Mulliken spin densities are more symmetric with respect to the center of the chain, but otherwise the results are quite similar. It can be shown that the delocalization for the planar model is more extended as it has been expected.

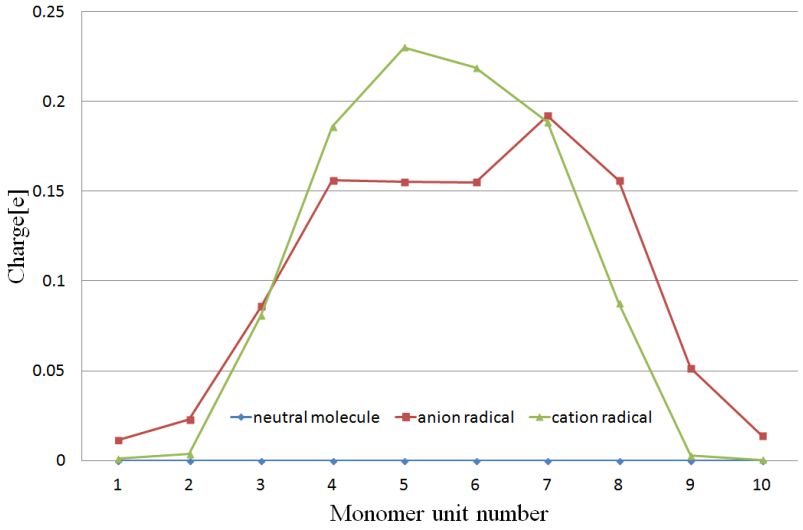

Figure 3.15: Summed Mulliken spin distributions on each monomer unit along the polymer backbone calculated by the DFTD method for the neutral molecule, anion radical and cation radical, respectively.

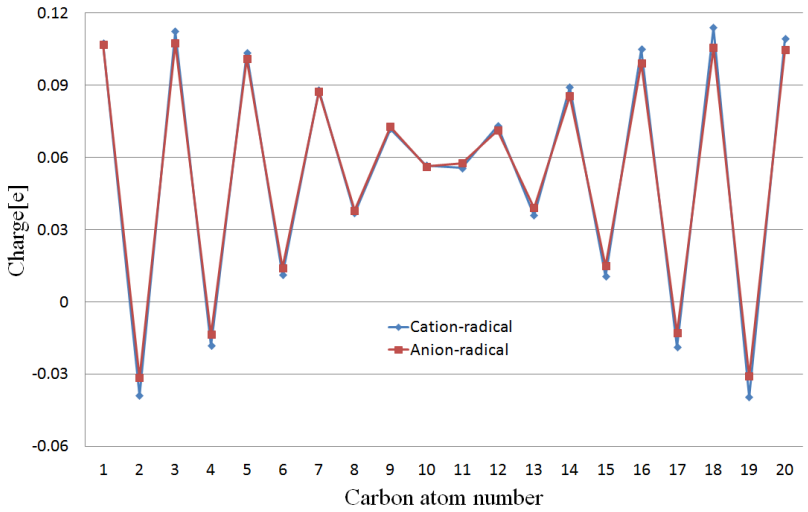

Figure 3.16: Mulliken spin distributions on carbon atoms along the planar acetylene calculated by the DFTD method.

3.2 Mutual position of two chains

Although there are more accurate approaches to the problem the solution of mutual position of two molecules we stayed only with the most basic one based on the Van der Waals radii of atoms. We assumed that our molecules are rigid bodies and each of their atoms is enclosed in a sphere with the radius equal to the Van der Waals radius of the respective atom. The approaching molecules can at most touch by the spheres. The Van der Waals radii were taken from the database of physical constants in the Mathematica software [21]. They are shown in Table 3.3.

Table 3.3: Van der Waals radii of atoms

Atom	Van der Waals radius
Hydrogen	120 pm
Carbon	170 pm
Silicon	210 pm

As the next step we searched for the minimal distance between the cation-radical and the anion-radical. The search for the minimal distance was programmed in the Mathematica software [21]. We did it in the following way. We took both molecules (cation-radical and the anion-radical) in the standard orientation of the Gaussian software [16]. Next we introduced a virtual axis passing through the middle of the polymer, around which the polymer backbone is twisted. This axis was chosen in such a way that it coincides with the Cartesian axis x in the standard orientation of the molecule in the Gaussian software [16]. We refer to this axis as a coordinate axis. As the final step we searched for the optimal position between the molecules which gave us the minimal distance between the coordinate axes of the molecules. Minimizing this distance is reasonable, because the initial step of the exciton dissociation is the creation of a CT state with the hole and the electron located at the adjacent molecules. This step is governed by the rate of the electron tunneling which depends on the tunneling distance. In order to maximize this tunneling rate we need to minimize the distance which the electron has to overcome. In the previous chapter we showed that the hole and the electron are located on the main backbone of the cation-radical and

anion-radical, respectively. This conclusion is based on the analysis of the Mulliken spin densities on both radicals. As a result we should minimize the distance between the main backbones. As a simplification of this procedure we decided to minimize the distance between the coordinate axes of the adjacent chains. Under the approximations mentioned above, our system of two molecules have six degrees of freedom, namely:
a) the distance between the molecules calculated as the distance between their coordinate axes,
b) the angle between the coordinate axes,
c) two rotations, each corresponding to the rotation of the molecule around its coordinate axis, and
d) two shifts, each corresponding to the shift of the molecule in the direction of the coordinate axis.

Table 3.4: The minimal distance between the axes for various angles

The angle between the coordinate axes	The distance between the coordinate axes
0 degrees	1455 pm
90 degrees	1305 pm
180 degrees	1459 pm
270 degrees	1284 pm

Searching for the minimal distance dependent on 5 variables (other degrees of freedom) is too difficult and we used the following simplifications. We took the angle between the coordinate axes as a parameter and limiting this parameter we looked for a solution only to several angles, namely, 0 degrees, 90 degrees, 180 degrees and 270 degrees. By this approach we decreased the number of variables to 4, but this is still not sufficient simplification for the solution of the problem. Next we found the minimal distance on the grid of 32×32 combinations of the angles corresponding to the rotations of the molecules around their respective coordinate axes and we retained the shift degrees of freedom fixed. On the grid the angles were varied by $\pi/16$ in the whole interval. After this optimal configuration had been found, we searched for the minimal distance on the grid of $3 \times 3 \times 15 \times 15$ combinations of the parameters. In this step the rotation degrees of freedom could change by $\pi/16$

from the optimal configuration from the previous step or it could remain the same. The shift degrees of freedom vary in the interval $[-70\,\mathrm{pm}, 70\,\mathrm{pm}]$ with the step of 10 pm. In Table 3.4 we show the minimal distances for the corresponding angles between the axes.

There were two reasons for choosing this approach. First, we wanted to have the best possible configuration of the chains to ensure proper calculation of the electric field generated by the anion-radical in the next step. Second reason was in limited computational resources which did not allow us to use more sophisticated procedures based on quantum-chemical calculations.

Chapter 4

Modeling of charge carrier photogeneration

In this chapter we present main results of our work in modeling the photogeneration of free charge carriers. First we present proposed changes to the Arkhipov model. Next we show how we introduced these changes into the model and, finally, we present the theoretical curves describing the photogeneration of free charge carriers in our model. The comparison of the new model to the previous one is at the end of this chapter.

4.1 Improvements to the Arkhipov model

In the modified Arkhipov model we changed the procedure how the potential for the electron-hole pair dissociation is calculated. Our new approach allowed us to eliminate two parameters of the original model which are connected exclusively with the calculation of the potential barrier. These parameters involve the initial separation distance d and the effective mass of the hole m_{eff}. By our approach we reduced the number of parameters of the model to only three, namely: the effective quantum yield η_{eff}, the relative permittivity ϵ_r and the preexponential factor A_{eff}.

The potential barrier in our model is calculated as a depth of the local potential well generated by the Coulomb interaction between the hole and the electron. The hole moves in the total electric field composed of the external electric field F and the electric field of the bound electron. The electric field

from the electron is calculated by the Gaussian software [16] taking the real distribution of the negative charge and the procedure is described below. Here the situation is different with respect to the Arkhipov model, where the electric field generated by the electron was calculated from the Coulomb potential of a localized electron. The external electric field is then added as an additive term. We obtained the electrostatic potential along the desired curve. We used two approaches:
a) we calculated the electrostatic potential along the line segment on the coordinate axes of the polymer molecule or a path along the bonds in the polymer backbone as an approximation of the real polymer backbone, or
b) we calculated the electrostatic potential along the bonds in the polymer backbone.
Then we could easily find local extremes of this electrostatic potential. The height of the potential barrier was calculated as a difference between the local maximum E_{max} and the local potential minimum E_{min}. As E_{max} we can take directly the local maximum of the electrostatic potential. As the minimum E_{min}, however, we did not take directly the local minimum of the electrostatic potential but we included the effects of delocalization of the hole as well. In the original model, the delocalization effect was introduced by the explicit assumption of the effective mass m_{eff} of the hole. Here, this was done in the following way. As E_{min} we took the minimum of the spectrum of the matrix $\mathbf{E}$, i.e. $E_{min} = \inf \sigma(\mathbf{E})$. The matrix $\mathbf{E}$ can be written as

$$\mathbf{E} = \begin{pmatrix} E_1 & \mathcal{T} & 0 & \cdots & 0 & 0 \\ \mathcal{T} & E_2 & \mathcal{T} & \ddots & 0 & 0 \\ 0 & \mathcal{T} & E_3 & \ddots & 0 & 0 \\ \vdots & \ddots & \ddots & \ddots & \ddots & \vdots \\ 0 & 0 & 0 & \ddots & E_{n-1} & \mathcal{T} \\ 0 & 0 & 0 & \cdots & \mathcal{T} & E_n \end{pmatrix} \tag{4.1}$$

where $\mathcal{T}$ denotes the transfer integral between the nearest sites on the polymer backbone, E_i denotes the energy of the i-th site and n denotes the number of sites among which the hole is delocalized. The energy of the i-th site is calculated as an average of the total electrostatic potential over the site. As the sites we chose monomer units. We considered that the hole is delocalized over all the sites with the energy lower than the energy of the local maximum of the total electrostatic potential. We note that instead of

the exact local maximum of the electrostatic potential we took the energy of the site with the highest energy. The reason is that we has to consider the potential of particular sites of the molecule. However, since the potential is slowly varying function, the results of the photogeneration of free charge carriers are not affected by such a approximation and it is physically reasonable to work with the same precision when calculating both E_{max} and E_{min}.

4.2 Electric field induced by the anion-radical

In this section we show how the electric field generated by the anion-radical was calculated. The calculations were done in the Gaussian software [16] using the command "Cube". There was only the anion-radical molecule considered for the calculation and the electric field was calculated at the point where the cation-radical is expected. We calculated the electric field by the DFTD method as described before. For comparison we also calculated the electric field by the HF method in the basis of atomic orbitals 6-31G*. First, we tried using an unrestricted version of the HF method. We found this approach not to be feasible, because of a large spin contamination. Hence, we had to use restricted open shell version of the HF method. This approach had still a problem with the convergence of the solution. We had to implement higher separation of energies of virtual and occupied orbitals along with limited convergence criteria. The convergence criteria were set two orders of magnitude below the default settings of the Gaussian software [16]. The main problem of the HF method was that it gave the energy of the highest occupied molecular orbital of the anion-radical to be above the energy of vacuum. Both methods (DFTD and HF) gave essentially the same electric potential generated by the anion-radical on the desired curve.

There is a question how to choose the set of points where we want the electric field from the negative charge to be calculated. We chose two different approaches although only one of them was found usable for solving our problem at the end. In the first approach we considered points along the coordinate axis of the cation-radical. In an alternative approach we took directly points along the bonds in the cation-radical.

First we tried to take the points along the line segment with the length of 3000 pm. The distance between the points on the line segment was 10

pm. In the second approach we considered the points along the bonds in the polymer backbone of the cation-radical dividing each bond to 14 equal intervals including the points corresponding to the location of the carbon atoms.

The problem with the second approach is that our calculations of the cation-radical molecule geometry was limited to 20 carbon atoms. Hence we were not able to describe the whole potential well which influences the charge pair dissociation. For that we would need to have the geometry of the cation-radical calculated for a longer chain. For this reason we had to use the first approach, using extrapolation with a prolonged line segment to 60000 pm. We preserved the distance between the test points on the line as 10 pm.

An example of the electric potential of the anion-radical, which was calculated along the line segment approximating the adjacent polymer chain, is shown in Figure 4.1 for the case when the cation-radical and anion-radical were antiparallel to each other. The distances between them were 1.5 nm, 1.6 nm, 1.7 nm and 1.8 nm respectively. The potential along the a real polymer chain is shown for the comparison. This potential was calculated for the distance between the chains 1.6 nm.

There is a question if we are able to model the electric potential calculated for a real distribution of charges in the anion-radical obtained from quantum-chemical calculations by a potential from a point charge, i.e. a single electron sitting on the adjacent chain as considered in previous models. The electric potential from an electron sitting as a point charge on the anion radical along the line approximating the cation-radical can be expressed as

$$\mathcal{U}(x) = \frac{-e}{4\pi\epsilon_0\epsilon_r\sqrt{b^2 + (x+c)^2}} \tag{4.2}$$

where ϵ_r corresponds to the relative permittivity, b corresponds to the distance of the electron from the line approximating the cation-radical and the last parameter c is a displacement of the potential minimum. We tried to fit the potential obtained by the previous calculations, in which we considered a real distribution of the charge in the anion-radical by this simplified case of taking a point charge potential. We took ϵ_r, b, and c as fitting parameters. We investigated how these parameters change depending on how many

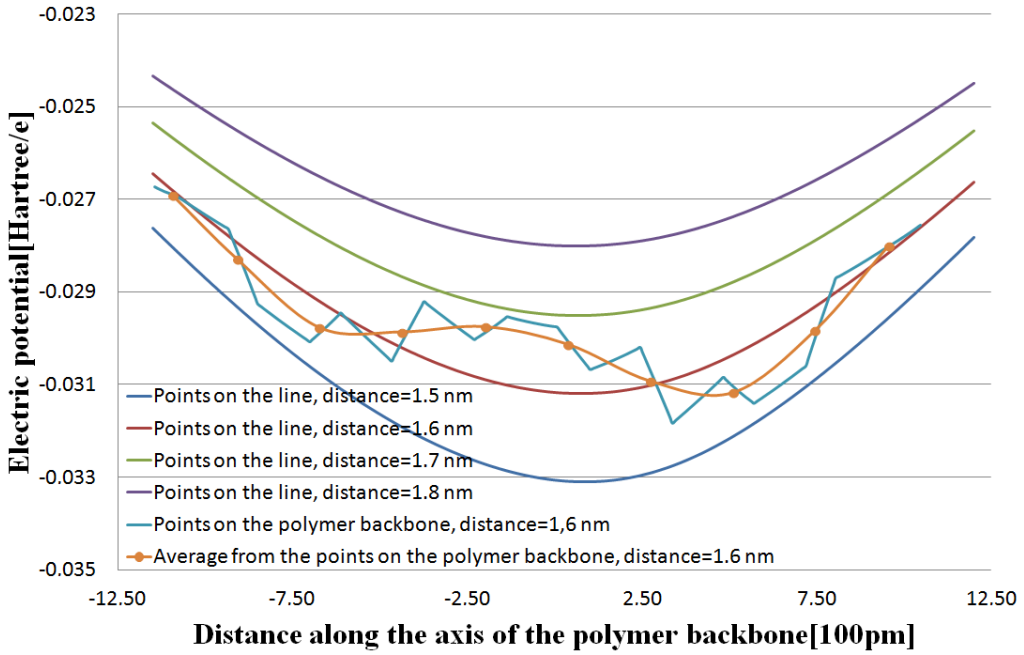

Figure 4.1: Electric potential generated by the anion-radical calculated along the line segment approximating the adjacent cation-radical (blue, red, green and purple curve, respectively), along the bonds in the cation-radical backbone (light blue curve) and electric potential along the bonds in the cation-radical backbone averaged to monomer units (orange curve).

points around the minimum we consider during the fit. When we are fitting less points of the electric potential, i.e. we are fitting only the close neighborhood of the minimum of the electric potential, we are able to describe the electric potential around the local minimum well. When we take more points we are able to describe the potential at the points further away from the local minimum of the potential correctly. However, we describe the electric potential around the minimum of the electric potential with a poor accuracy only. The relations of the fitted parameters on the number of fitted points can be seen in Figures 4.2-4.4. In these figures the red curve corresponds to 0 degree angle between the cation-radical and anion-radical, the blue one to the 90 degree angle, the green one to the 180 degree angle and the brown one to the 270 degree angle. In all the figures we can see that when the polymers are orthogonal to each other there is only a slight dependence of

the fitted parameters on the number of points considered in the fit. The situation is different for the case of parallel radicals. This means that for the case of the orthogonal chains we are essentially able to describe the electric potential calculated for the charge distribution on the anion-radical by the electric potential of the single electron charge. For the case of parallel chain however, we are not able to do so. This is caused by the behavior of the calculated electric potential for the charge distribution on the anion-radical around its minimum.

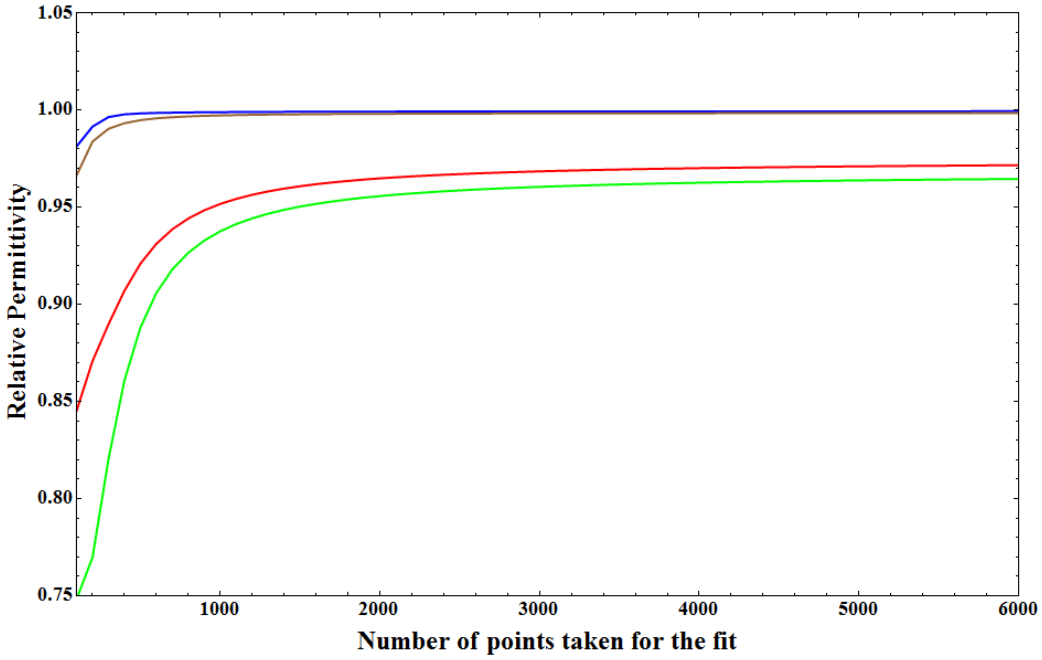

Figure 4.2: The dependence of the fitted relative permittivity on the number of points taken for the fit of the electric potential calculated for different angles between the polymers: 0 degrees (red curve) for , 90 degrees (blue curve) for , 180 degrees (green curve) and 270 degrees (brown curve).

In Figure 4.2 we see the dependence of the fitted relative permittivity on the number of fitted points. As we mentioned earlier for the degrees 90 and 270 there is only a slight dependence. The dependence for the degrees 0 and 180 is much larger. We can see that when we want to describe the local minimum correctly we need to use unrealistic values of relative permittivity

which is around $0.75 - 0.9$. Also it can be seen that for the parallel case even for the large number of fitted points we do not get close to the realistic value of the relative permittivity equal to 1.

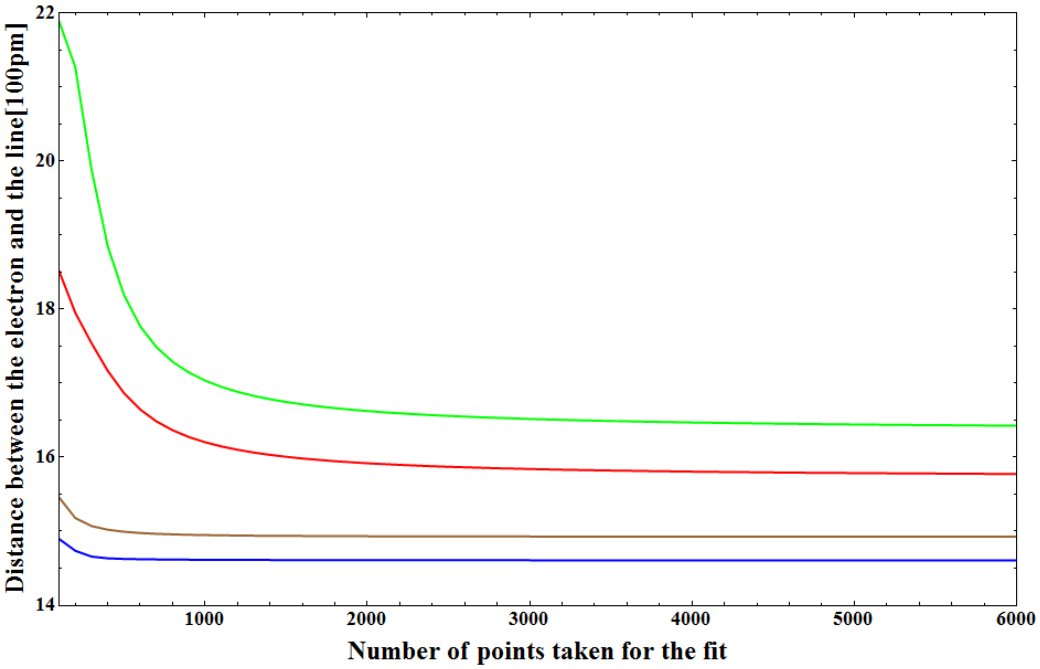

Figure 4.3: The dependence of the fitted distance of the electron from the coordinate axis of the adjacent polymer on the number of points taken for the fit of the electric potential calculated for different angles between the polymers: 0 degrees (red curve) for , 90 degrees (blue curve) for , 180 degrees (green curve) and 270 degrees (brown curve).

In Figure 4.3 we see the dependence of the fitted distance of the electron from the coordinate axis of the adjacent chain on the number of fitted points. We can see again that for the angles 90 degrees and 270 degrees there is almost no dependence of this variable. However for the 0 degrees and 180 degrees the distance of the electron and the line changes quite significantly. It is worth mentioning that the obtained distances are unrealistic for several reasons. The first reason is that this distance should enable the electron tunneling between the chains during the transformation of the exciton and such high distances, as we obtained for a bounded electron-hole pair, would

not allow this transformation. Another reason is that the distance between the axes of the anion-radical and the cation-radical calculated in the previous chapter are smaller than those obtained by this fit. For the convenience we list them in Table 4.1. *Angle* denotes the angle between the coordinate axes of the adjacent polymer chains, *Distance* denotes calculated distance between the coordinate axes of the polymer chains, *Minimum* and *Maximum* denotes the minimum of the fitted distance between the axis and the electron and the maximum of this distance, respectively.

Table 4.1: Distance between the axes and the fitted distance for various angles

Angle[degrees]	*Distance*[pm]	*Minimum*[pm]	*Maximum*[pm]
0	1455	1577	1851
90	1305	1461	1490
180	1459	2188	1643
270	1284	1493	1546

In Figure 4.4 we can see the dependence of the displacement coefficient on the number of fitted points. One can see that this is essentially independent on the number of fitted points. This is an expected result because this parameter gives us the position of the minimum of the potential.

The last Figure 4.5 shows two fits of the electric potential calculated for the antiparallel polymer chains (180 degrees between the coordinate axes of two polymer molecules.) The curve calculated from the charge distribution on the anion-radical is red. The blue dashed curve is the fit for the 301 points. The black dashed curve is the fit for the whole interval, i.e. all the 6001 points. We can see that the blue curve describes the minimum of the potential almost perfectly, but fails for large distances. The black curve describes large distances well but fails around the minimum of the potential.

We can conclude that the electric potential generated by the anion-radical can not be satisfactory estimated by the Coulomb potential of a single charge for the case of parallel and antiparallel chains. The reason for this is that

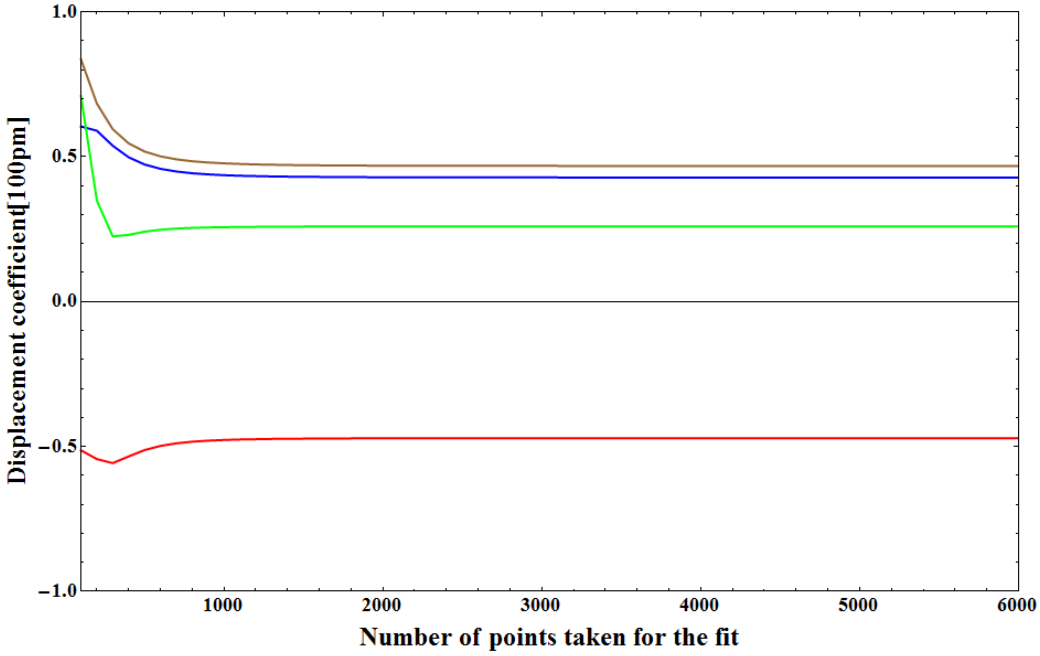

Figure 4.4: The dependence of the fitted displacement coefficient on the number of points taken for the fit of the electric potential calculated for the different angles between the polymers (red curve for 0 degrees, blue curve for 90 degrees, green curve for 180 degrees and brown curve for 270 degrees).

we would have to use physically unrealistic parameters, namely relative permittivity would have to be smaller than one and also the initial separation distance is too large. For the case of orthogonal chains we can estimate a potential by the Coulomb potential of a single charge, but still we would have to use unrealistically large initial separation distance of the CT state.

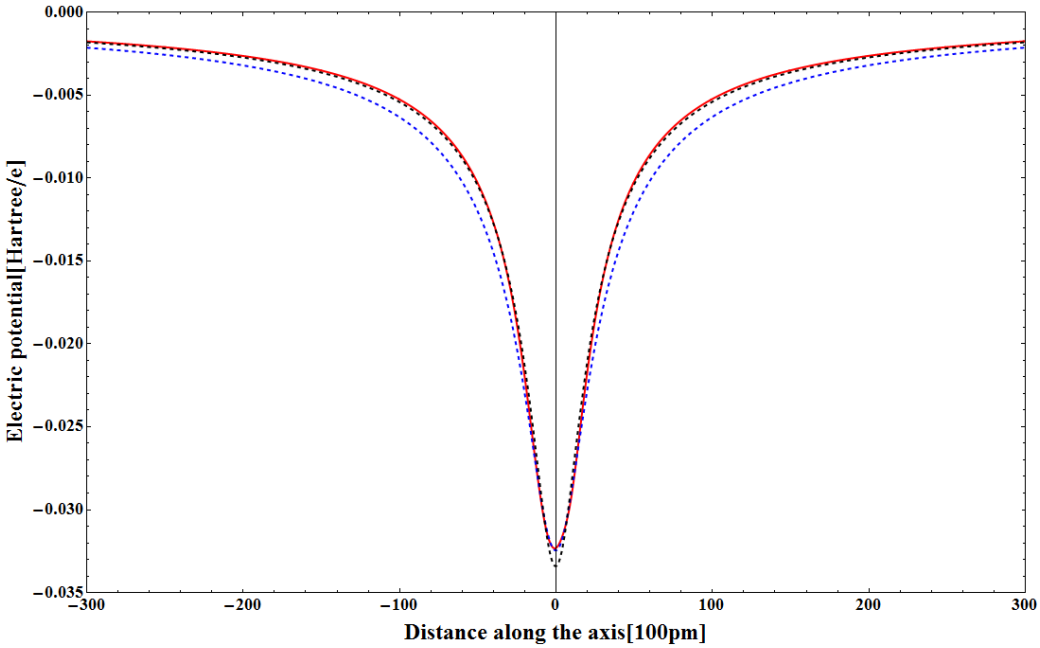

Figure 4.5: Electric potential calculated for the antiparallel polymer chains fitted by the Coulomb law. The red curve corresponds to the electric potential calculated from the charge distribution on the anion-radical. The blue dashed curve is the fit of the Coulomb law for 301 points around the minimum of the potential. The black dashed curve is the fit of the Coulomb law for 6001 points around the minimum of the potential.

4.3 Calculation of the transfer integral

The calculation of the transfer integral is done in the same way as described in [22]. We took a segment consisting of two monomer units from the middle of the cation-radical. We end-capped this segment with hydrogen atoms. For this system we calculated the energy of the highest occupied molecular orbital E_+ and the energy of the second highest occupied molecular orbital E_-. In the next step we divided this dimer to two monomer units. Hydrogen atoms were added to both these monomer units to end-cap the broken bonds and the energy of the highest occupied molecular orbital was calculated for both monomers separately. We denote these energies as E_1 and E_2. The

transfer integral can be then calculated according to [22] as

$$\mathcal{T} = \frac{1}{2}\sqrt{(E_+ - E_-)^2 - (E_1 - E_2)^2}. \tag{4.3}$$

The calculation of the orbital energies was done using the Gaussian software [16]. For this calculation we used the HF method with the atomic orbitals basis 6-31G*. This approach was successfully used for the calculation of the transfer integral in poly(phenylenevinylene) and in polythiophene [23].

This approach can be done only under the assumption that the highest occupied molecular orbital of the dimer is a linear combination of the highest occupied molecular orbitals of the monomer units. We can at least partially check the validity of this assumption in two ways. The first possibility is to look directly at the shape of the orbitals under consideration. The second option is to look at the behavior of the energy of the two highest occupied molecular orbitals of the dimer when we prolong the bond connecting them. They should converge to the energy of the highest occupied molecular orbital of the independent monomer units. Because we consider the same monomer units their energies are essentially the same. This behavior can be seen in Figure 4.6. Both of these approaches leads to the conclusion that our assumption about the highest occupied molecular orbital of the dimer was correct. The transfer integral obtained by this approach has the value $\mathcal{T} = 0.3160eV$.

We also studied the dependence of the transfer integral on the dihedral angle between the monomer units. Possible angles are quite limited because during this calculation we froze other degrees of freedom and also the side groups restricted the motion. The calculated values can be seen in Figure 4.7. In this picture we can see that surprisingly by narrowing the angle we do not obtain a bigger transfer integral. The reason for this strange behavior could be found in the interaction between the side groups. The side groups are quite close to each other. The distance between them is approximately 300 pm. This explanation can be justified when one looks at the highest occupied molecular orbital which spreads also partially on the side groups.

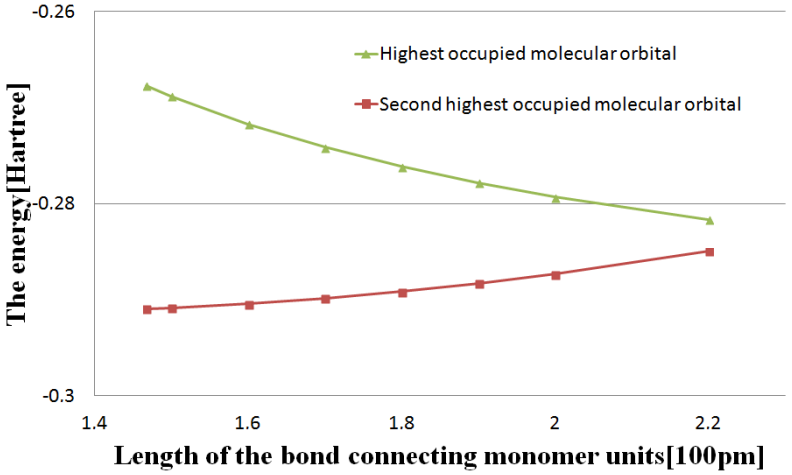

Figure 4.6: The dependence of the energy of the highest occupied orbitals of the dimer on the connecting bond length.

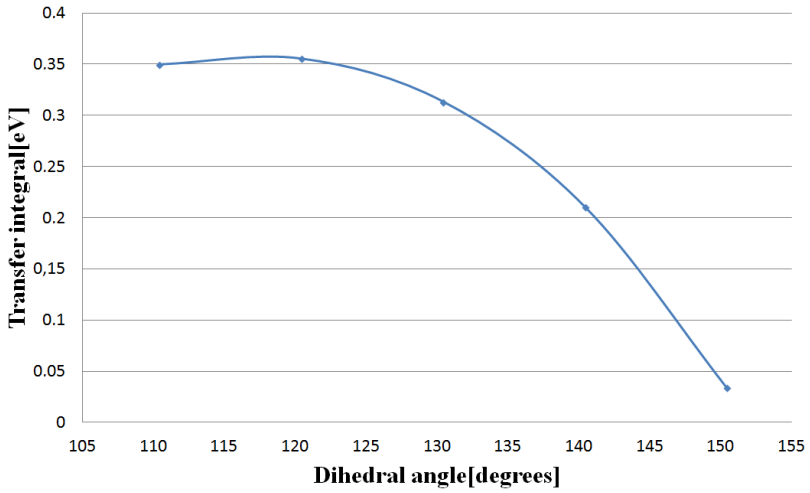

Figure 4.7: The dependence of the transfer integral on the dihedral angle between two monomer units.

4.4 Potential barrier

In this section we describe the procedure used for the calculation of the height of the potential barrier. In the previous section we described the procedure how we obtained a set of points along the adjacent polymer backbone with the electric potential of the anion-radical. In order to calculate the dissociation of charge-pair, we added to this potential the term describing the effect of the external electric field. This term corresponding to the electric potential energy can be written as

$$U_F(\vec{x}) = e\vec{F} \cdot \vec{x} \tag{4.4}$$

where $\vec{x}$ is the positional vector , $\cdot$ denotes the standard scalar product in $\mathbb{R}^3$ and $\vec{F}$ is the vector of the external electric field. The vector of the homogeneous electric field $\vec{F}$ can be expressed in spherical coordinates as

$$\vec{F} = F(\cos(\phi)\cos(\theta), \sin(\phi)\cos(\theta), \sin(\theta)) \tag{4.5}$$

where F denotes the absolute value of the electric field and $\theta \in (-\pi/2, \pi/2)$, $\phi \in [0, 2\pi)$ determine the angles of the vector of the electric field in the spherical coordinates. We denote $U_e(\vec{x})$ as the electric potential generated by the anion-radical in the point with the position vector $\vec{x}$. The total electric potential energy can be calculated as

$$U(\vec{x}) = U_F(\vec{x}) + \frac{e\mathcal{U}_e(\vec{x})}{\epsilon_r}. \tag{4.6}$$

We added the relative permittivity in this way to emulate the effect of the surrounding material. The dielectric constant was introduced into this formulae because the previous calculation of the electric potential generated by the anion-radical was done for the isolated molecule in vacuum, however in the real material the cation-radical and anion-radical are surrounded by other molecules which form a polarizable medium.

Now we have to average this total potential over the sites corresponding to the monomer units. The reason for this is that we have the transfer integral calculated between the two neighboring monomer units. We calculated the electric potential along the line segment on the coordinate axis. We had to find the way how to assign 6001 points on the coordinate axis to the sites corresponding to the monomer units. As we mentioned earlier one site is

composed from one monomer unit. The points along the bonds in the polymer backbone can be assigned to the sites in the following way. We say that one site includes all the points on one double bond of the monomer unit and of the points on one half of the single bond connecting the monomer unit to the previous and the next monomer unit.

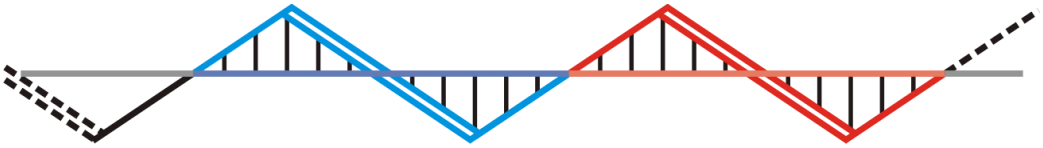

Figure 4.8: Assignment of the points on the line segment to the sites corresponding to the monomer units.

In Figure 4.8 we see this assignment schematically. One "site" is marked blue and the other one red. After assigning the points on the polymer backbone to the particular sites we projected these points orthogonally to the coordinate axis as sketched by the black lines in Figure 4.8. By this approach we defined the line segments on the coordinate axis. These line segments correspond to the sites in the polymer backbone. This procedure defined the sites for the points "inside" the decamer. However, we need to assign also the points "outside" the decamer. After careful analysis we found that the line segments representing the polymer sites on the coordinate axis have lengths sequentially as 240 pm, 240 pm and 230 pm. These lengths repeat periodically. Adopting this approach we were able to define virtual sites even behind the range of the model decamer. Next we averaged the total potential energy obtained according to the equation 4.5 over the points belonging to each particular site. On this averaged total potential we were able to find the local maximum E_{max}, local minimum E_{minim} and the potential well along the polymer chain. The latter should be distinguished from the value E_{min} obtained as the minimal eigenvalue of the matrix $\mathbf{E}$, which takes into the account the effect of delocalization due to transfer integrals. Under the local maximum E_{max} we understand the local maximum of the averaged total potential of some inner site. If the local maximum of the averaged total potential corresponds to the site at the end of the line segment we do not consider it as the local maximum E_{max}. As a potential well we take the neighboring sites with the energy lower than the one of the local maximum E_{max} in the direction of the local minimum E_{minim}. There are several cases

how the situation on the line can look like. We have to assign the height of the potential barrier to each one of the following cases:
a) we are able to find both the local minimum E_{minim} and the local maximum E_{max}, and the potential well is located over more than one site,
b) we are able to find both the local minimum E_{minim} and the local maximum E_{max}, and the potential well is spread over one site, which coincides with the local minimum E_{minim},
c) we are able to find only the local minimum E_{minim}, and
d) we are not able to find neither the local minimum E_{minim} nor the local maximum E_{max}.

We just briefly skim through the situations b)-d) to explain when they can occur. The case d) happens when the external electric field is not orthogonal to the polymer axis and it is large enough to overcome the potential well generated by the Coulomb interaction to such a degree that there is no bound state. Under such a regime each CT state would dissociate into free charge carriers. Such situation was highly improbable in the original model. We will show that in our model this situation can happen more probably than in the original model, because the potential well calculated by quantum calculation is more shallow than that one calculated using classical approach. The case c) corresponds to the situation when the electric field is orthogonal to the polymer chain or it is not large enough to overcome the Coulomb interaction in the range of our test points. The case b) represents the transition between the cases a and d). For all the cases we assigned the height of the potential barrier ΔE in the following way:
a) $\Delta E = E_{max} - E_{min}$, where $\mathbf{E}$ is the matrix denoted by (4.1) and we take all the sites from the potential well as a diagonal elements of the $\mathbf{E}$,
b) $\Delta E = E_{max} - E_{minim}$,
c) $\Delta E = \min(U(\vec{x}_{min}), U(\vec{x}_{max})) - E_{min}$, where $\min(U(\vec{x_{min}}), U(\vec{x_{max}}))$ is the minimum taken from the endpoints of the averaged total potential generated by the anion-radical and we take all the sites with the energy lower than $\min(U(\vec{x}_{min}), U(\vec{x}_{max}))$ as a diagonal elements of the matrix $\mathbf{E}$, and
d) $\Delta E = 0$.

In Figures 4.10 and 4.9 we show the dependence of the local maximum E_{max} and the energy minimum $E_{min} = \inf(\sigma(\mathbf{E}))$ on the electric field for the case, in which the angle between the coordinate axes of the polymer chains is 0 degree. The different colors correspond to different values of relative permittivity. Red color corresponds to the value $\epsilon_r = 1$, blue color to the

value $\epsilon_r = 2$, green color to the value $\epsilon_r = 3$ and brown color to the value $\epsilon_r = 4$. It can be seen that the main dependence of the exponent ΔE comes from the change of the local maximum E_{max}, because the energy minimum is almost independent on the external electric field. This is caused by the fact that there is a large effect of the delocalization of the hole.

In Figure 4.9 we see that for the high electric fields there is a steep increase, which is caused by the decrease of the number of sites taken into the diagonalization process. Essentially we can say that each step on the graph corresponds to the decrease of the number of sites by one. This behavior is a direct result of the discrete sites structure of our model. The moment when the minimal energy increases to zero value corresponds to the situation d) from above, i.e. no minimum occurs. We note that in the original model the critical value of the electric field when the situation d) occurs was estimated as $4 \cdot 10^7 - 1 \cdot 10^8$ V [2]. For the case of the relative permittivity $\epsilon_r = 3$ or $\epsilon_r = 4$ we obtain similar critical fields.

In Figure 4.10 there is a discontinuity for high electric fields, which corresponds to the situation d), similarly as in the previous case. We note that for the low electric field limit we underestimate the local maximum E_{max}. The reason is that this situation corresponds to the case c) from above. In this case we take the value which is lower that the actual local maximum E_{max}. We note that for the electric field equal to 0, the local maximum should be equal to 0. As a result we slightly overestimate the total quantum yield of the photogeneration of free charge carriers η for the low electric field limit.

Now we are finally ready to calculate the total quantum yield of the photogeneration of free charge carriers.

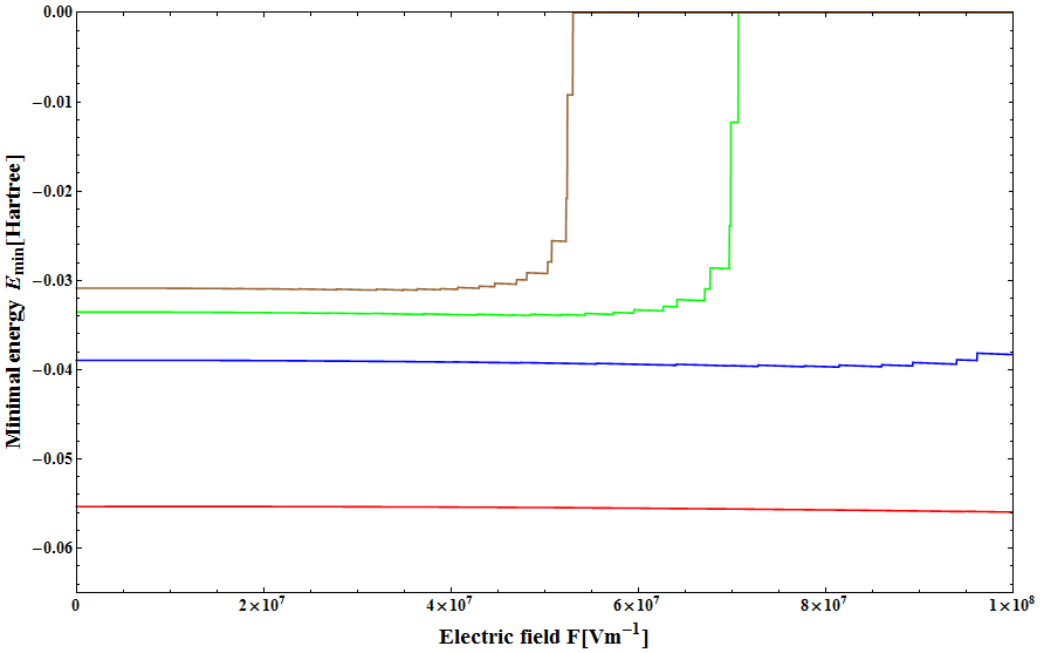

Figure 4.9: The dependence of the energy minimum E_{min} on the intensity of the external field projected in the direction of the coordinate axis calculated from the total potential for the case of the parallel chains. The different colors corresponds to the different permittivities: $\epsilon_r = 1$ (red curve), $\epsilon_r = 2$ (blue curve), $\epsilon_r = 3$ (green curve) and $\epsilon_r = 4$ (brown curve).

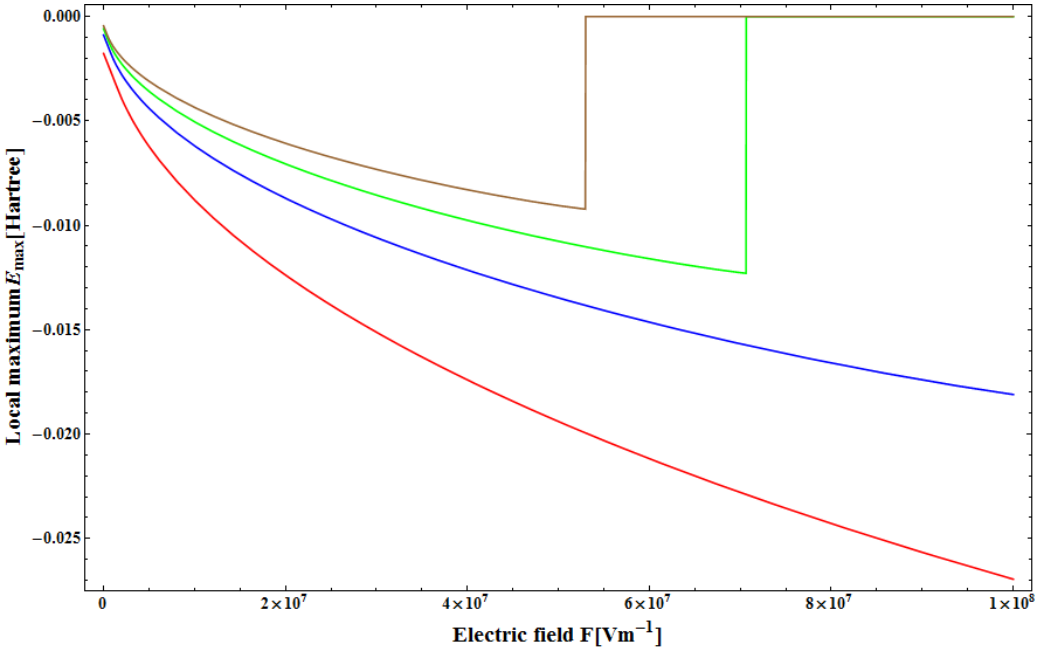

Figure 4.10: The dependence of the local maximum E_{max} on the intensity of the external field projected in the direction of the coordinate axis calculated from the total potential for the case of the parallel chains. The different colors corresponds to the different permittivities: $\epsilon_r = 1$ (red curve), $\epsilon_r = 2$ (blue curve), $\epsilon_r = 3$ (green curve) and $\epsilon_r = 4$ (brown curve).

4.5 Test curves of the new model

In the previous sections we described the procedure how we obtained the total quantum yield of the photogeneration of free charge carriers for a fixed combination of the angles θ and ϕ corresponding to the particular direction of the electric field with respect to the test line. In a real system the polymer chains are randomly oriented and as a result we need to average the total quantum yield of the photogeneration of free charge carriers with respect to the angles θ and ϕ. We did it in the following way

$$\eta(F) = \frac{1}{110} \sum_{i=1}^{11} \sum_{j=1}^{10} \cos\left(-\frac{\pi}{2} + (i-1)\frac{\pi}{10}\right) \eta\left(F, -\frac{\pi}{2} + (i-1)\frac{\pi}{10}, (j-1)\frac{\pi}{5}\right) \tag{4.7}$$

where $\eta(F,\theta,\phi) = \eta_{eff}\frac{1}{1+A_{eff}exp(\frac{\Delta E}{kT})}$ denotes the total quantum yield of the photogeneration of free charge carriers for fixed F, θ and ϕ. For our further calculation we have precalculated the values of the potential barrier ΔE for certain set of points $(F, \theta, \phi, \epsilon_r)$. Our model has two tunable parameters, namely the preexponential factor A_{eff} and the effective primary quantum yield η_{eff}. There is another parameter which is the relative permittivity of the material ϵ_r.

For the following discussion of the effects of the parameters on the total quantum yield we rewrite the previous expression in the logarithmic scale as

$$\log \eta(F) = \log\left(\frac{\eta_{eff}}{110}\right) + \log\left(\sum_{\theta,\phi} \cos(\theta) \frac{1}{1 + A_{eff} \exp(\frac{-E_{min}}{kT}) \exp(\frac{E_{max}}{kT})}\right) \tag{4.8}$$

We can easily see that in the logarithmic scale the effective primary quantum yield η_{eff} only shifts the total quantum yield vertically. We note that $\eta_{eff} \in [0, 1]$. The shape of the curve is dependent only on the preexponential factor A_{eff} and on the relative permittivity ϵ_r. The relative permittivity of the material can be measured and as a result only one parameter can be chosen truly arbitrarily - the preexponential factor A_{eff}.

If we consider the relative permittivity to be also a fitting parameter, we could try to find its values for the best fit of the experimental data obtained previously [2], using four different values of ϵ_r, namely $1, 2, 3$ and 4. We

obtained that the best fit for $\epsilon_r = 3$, which corresponds to the relative permittivity of our material obtained by independent measurements quite well. Eventually, we were able to use relative permittivity equal to 4, however such fit of the experimental data gave worse results for the low electric field limit compared to the relative permittivity 3. For the relative permittivity 1 and 2 we were not able to find a suitable set of parameters A_{eff} and η_{eff} which describe experimental data satisfactory.

The preexponential factor A_{eff} essentially compensates for the large term $\exp(\frac{-E_{min}}{kT})$. If we look at the size of the exponent $\frac{-E_{min}}{kT}$ we obtain for the temperature $T = 300K$ a number around $30 - 50$ depending on the relative permittivity. Such a large number in the exponent has to be compensated by the preexponential factor equal to $A_{eff} = 10^{-10} - 10^{-21}$.

In Figure 4.11 we present the fits of the experimental data. For different angles between the coordinate axes of the adjacent polymer chains. In Table 4.2 the parameters of the curves are summarized.

Table 4.2: Fitting parameters of the curves shown in Figure 4.11 for $\epsilon_r = 3$

Angle[degrees]	Curve	A_{eff}	η_{eff} [e/photon]
0	red	10^{-12}	0.005
90	blue	$0.5 \cdot 10^{-12}$	0.0047
180	green	10^{-12}	0.004
270	brown	$0.5 \cdot 10^{-12}$	0.004

All the curves were calculated with the same relative permittivity $\epsilon_r = 3$. We can see that for each angle we were able to fit the experimental data quite well. There is only a slight overestimation of the total quantum yield for the low electric field limit, which is caused by underestimating the local maximum E_{max} as described above.

Figure 4.12 shows another fit of the experimental data using the relative permittivity $\epsilon_r = 4$. Again, the different curves corresponds to the different angles between the coordinate axes of the polymer chains. Table 4.3 summarizes the parameters of the curves.

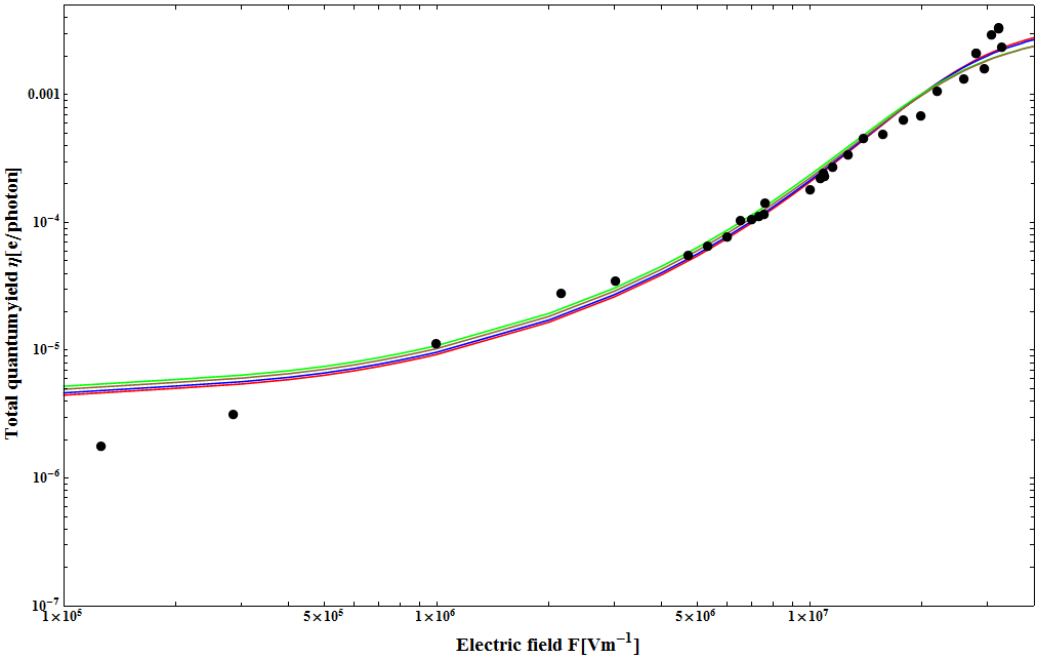

Figure 4.11: The model curves for the total quantum yield of the photogeneration of free charge carriers with the measured experimental data for $\epsilon_r = 3$. The different colors corresponds to the different angles: 0 degrees (red curve), 90 degrees angle (blue curve), 180 degrees angle (green curve), 270 degrees angle (brown curve).

Table 4.3: Fitting parameters of the curves shown in Figure 4.12 for $\epsilon_r = 4$

Angle[degrees]	Curve	A_{eff}	η_{eff} [e/photon]
0	red	10^{-10}	0.0047
90	blue	$0.5 \cdot 10^{-10.5}$	0.0025
180	green	$10^{-10.5}$	0.0012
270	brown	$0.5 \cdot 10^{-10}$	0.006

We can see that using higher permittivity we are able to describe the photogeneration of free charge carriers to some degree better in the high electric

field limit, however the problematic low electric field limit is worse than for the case of relative permittivity 3.

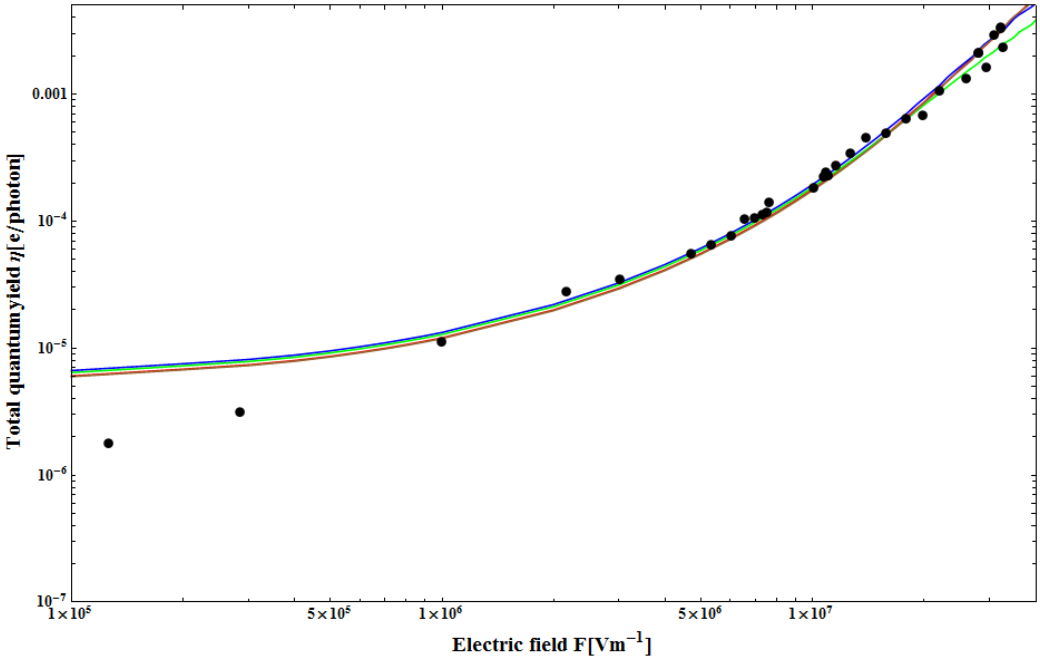

Figure 4.12: The model curves for the total quantum yield of the photogeneration of free charge carriers with the measured experimental data for $\epsilon_r = 4$. The different colors corresponds to the different angles: 0 degrees (red curve), 90 degrees angle (blue curve), 180 degrees angle (green curve), 270 degrees angle (brown curve).

4.6 Benefits of the new model

In this section we compare the previous model with our proposed one. A detailed analysis of the previous model showing its limits was given in [3]. The first difference of our model compared to the previous one is in the number of parameters. There are five parameters in the original Arkhipov model, namely effective primary quantum yield η_{eff}, preexponential factor A_{eff}, relative permittivity ϵ_r, initial separation distance d and effective mass

of the hole m_{eff}. The new proposed model uses only three parameters. By the different approach to the calculation of the potential barrier we are able to eliminate the parameters d and m_{eff}.

It has been shown that for the correct description the experimental data of the quantum yield of the photogeneration of free charge carriers within the previous model we need to model experimental data in several regions of the electric field separately with different parameters. The parameters of the previous model, with the exception of the parameter d and m_{eff}, differed quite substantially between the different regions of the electric field. The most problematic issue was the necessity of using different relative permittivities in different regions of the applied electric field. In the proposed model we are able to fit the experimental data on the whole interval of the applied electric field in the experiment with only one set of parameters η_{eff}, A_{eff} and ϵ_r.

In Figure 4.13 we compare the energy of the local maximum calculated in the original and new model. The new model is represented by the full lines and the curves from the older Arkhipov model are dashed lines. For this graph we chose the angle between the axes of the chains to be 0 degrees. The different colors correspond to the different relative permittivities, namely the red curve $\epsilon_r = 1$, the blue curve $\epsilon_r = 2$, the green curve $\epsilon_r = 3$ and the brown curve $\epsilon_r = 4$. The one remaining parameter of the original model was chosen as $d = 1.6$ nm. We can see that the original model is able to calculate the local maximum quite well even at the high electric field when the bound state disappears. The only problem is that we chose the initial separation distance according to the fit of the Coulomb interaction in the previous section. For the original model such high initial separation distance would be hard to explain, because it is assumed that this is the distance which the electron has to overcome by the tunneling mechanism.

In Figure 4.14 we can see the minimal energy E_{min} of the trapped hole for the new model and for the previous one. Unlike the local maximum, there are a quite large difference. The colors of the curves correspond to different relative permittivities in the same way as in Figure 4.13. The parameters for the original model were chosen as $d = 1.6$ nm and $m_{eff} = 0.1\ m_e$. The curves of the new model were calculated for the angle 0 degree between the coordinate axes of the adjacent polymer chains. The profile of the minimal

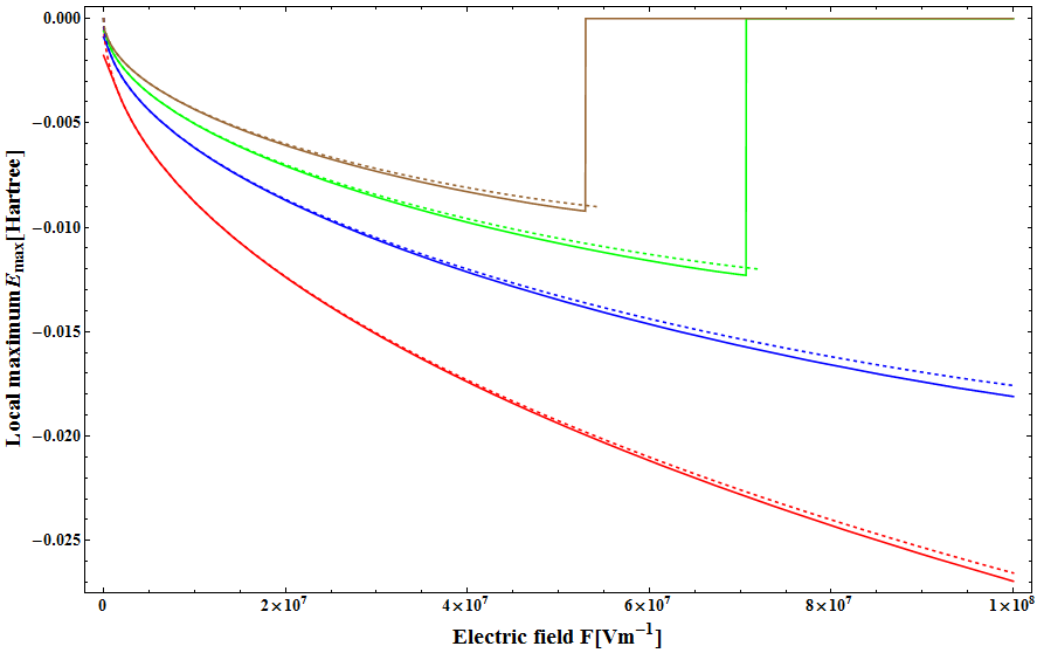

Figure 4.13: The dependence of the local maximum E_{max} on the external electric field projected in the direction of the coordinate axis compared to the original model(dashed curves). The different colors corresponds to the different permittivities: $\epsilon_r = 1$ (red curve), $\epsilon_r = 2$ (blue curve), $\epsilon_r = 3$ (green curve) and $\epsilon_r = 4$ (brown curve).

energy for the new model is quite different from the one in the original model. The main difference of the both models can be found in the respective dependence of the minimal energy E_{min} on the external electric field. We note a significant vertical shift of the energy minimum E_{min} for high electric fields, particulary for higher relative permittivities.

As the old model could not explain this vertical shift of E_{min} for high electric fields, it had to be corrected by artificially introducing the dependence of the constant A_{eff} on the external electric field.

In Figures 4.15-4.17 we compare the overall quantum yield of free charge carrier photogeneration calculated by the previous Arkhipov model [3] and by our new model. Since it was not possible to fit the experimental data by

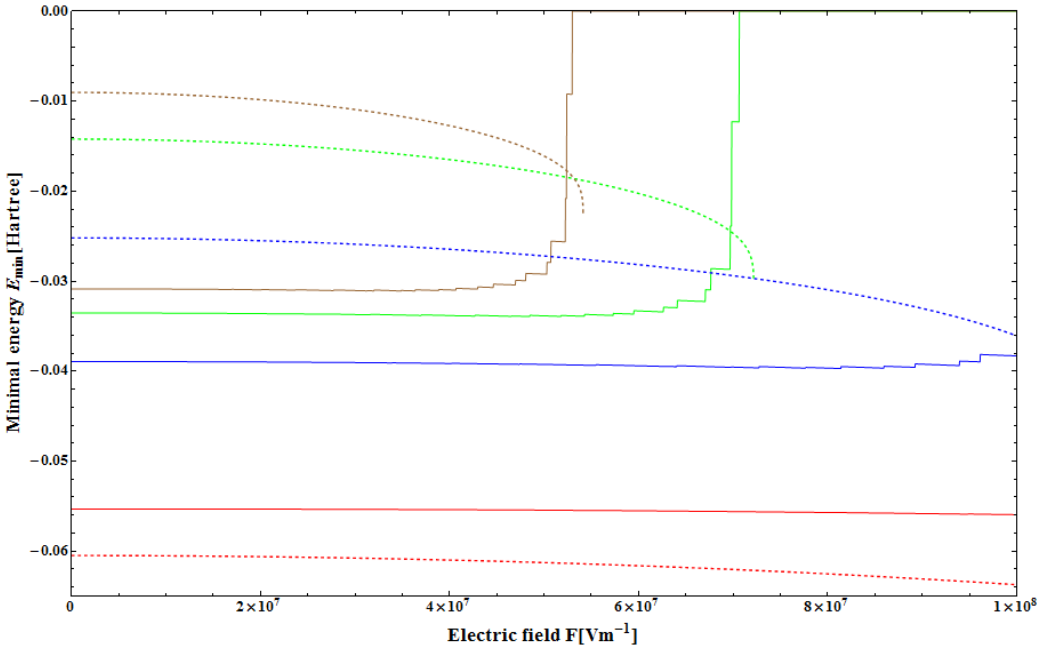

Figure 4.14: The dependence of the energy minimum E_{min} on the external electric field projected in the direction of the coordinate axis compared to the original model(dashed curves). The different colors corresponds to the different permittivities: $\epsilon_r = 1$ (red curve), $\epsilon_r = 2$ (blue curve), $\epsilon_r = 3$ (green curve) and $\epsilon_r = 4$ (brown curve).

the previous Arkhipov model on the whole interval of the applied electric field we have to compare the fits for three intervals separately. We can easily see that our model fits experimental data much better than the original one. In the following figures orange curve represents fit of our new model for $\epsilon_r = 3$ and the purple one for $\epsilon_r = 4$. In Figure 4.15 we have the low electric field limit fit for the previous Arkhipov model, in Figure 4.16 we have the fit for the middle-high electric field and in Figure 4.17 we have the fit for the high electric field limit.

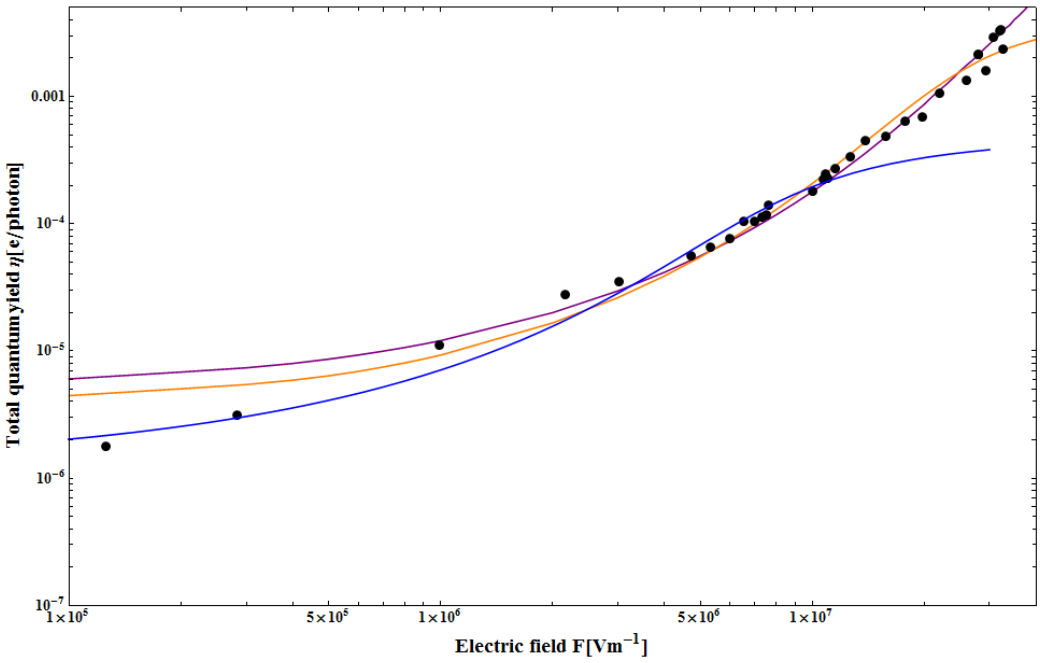

Figure 4.15: The comparison of the total photogeneration quantum yield calculated within the modified Arkhipov model on the applied electric field (blue curve) and within our new model for the $\epsilon_r = 3$ (orange curve) and for the $\epsilon_r = 4$ (purple curve).

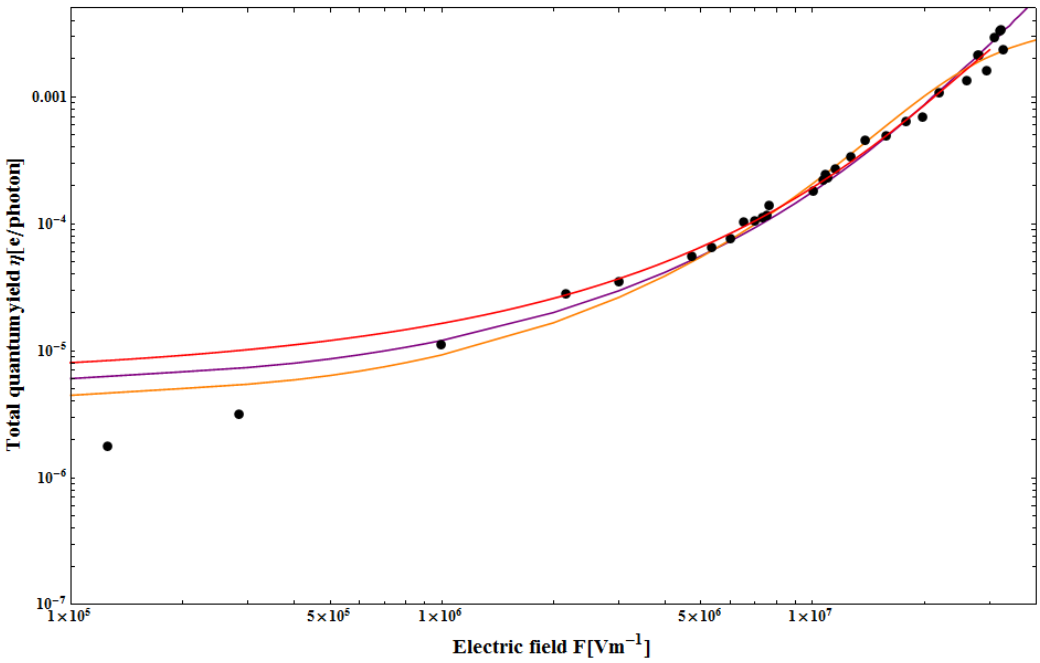

Figure 4.16: The comparison of the total photogeneration quantum yield calculated within the modified Arkhipov model on the applied electric field (green curve) and within our new model for the $\epsilon_r = 3$ (orange curve) and for the $\epsilon_r = 4$ (purple curve).

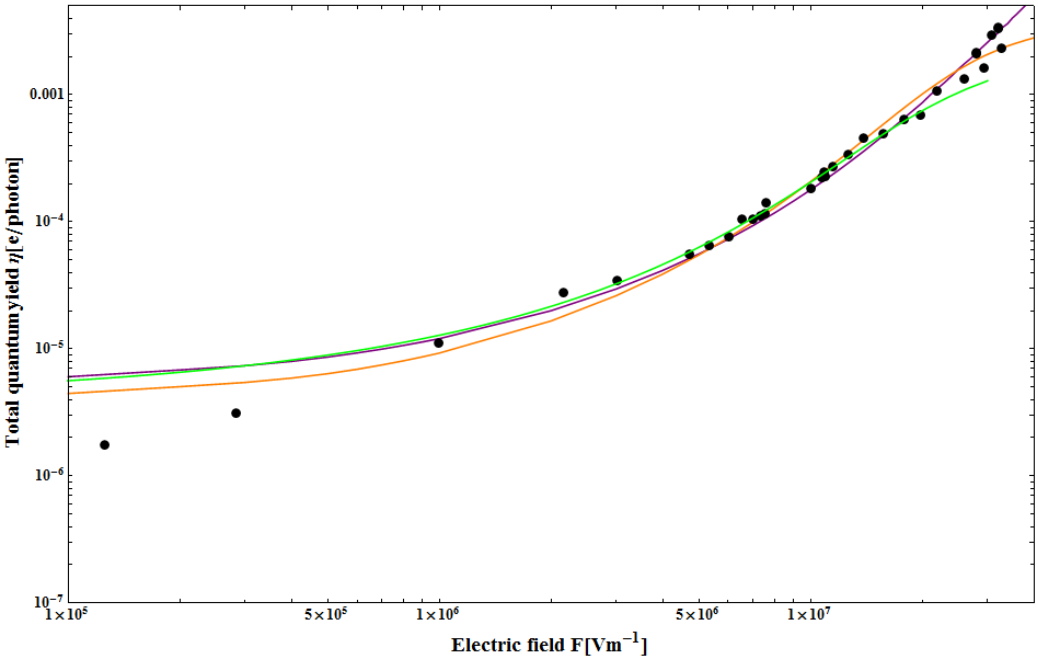

Figure 4.17: The comparison of the total photogeneration quantum yield calculated within the modified Arkhipov model on the applied electric field (red curve) and within our new model for the $\epsilon_r = 3$ (orange curve) and for the $\epsilon_r = 4$ (purple curve).

Chapter 5

Conclusion

In this work we have proposed further improvements to the Arkhipov model presented in [1] and revisited in [2, 3]. We studied the photogeneration of free charge carriers in [1-trimethylsilylphenyl,2-phenyl]acetylene. We used different approach to the calculation of the potential barrier in the model. The potential generated by the interaction between the anion-radical and the hole was calculated by quantum-chemical methods. The energy minimum for the hole was calculated as a ground state of the system with discrete number of interconnected sites connected with their mutual interaction given by the transfer integrals. This approach allows us to reduce the number of parameters from 5 to 3. the proposed model is capable to model the experimental data using only one set of parameters for the whole interval of the external electric field. The only drawback of our model is the necessity to calculate the optimal geometry of the anion-radical and the cation-radical for the studied material.

The overall quantum yield of the photogeneration of free charge carriers was calculated for various configurations of the anion-radical and the cation-radical. For all these configurations a set of parameters modeling the experimental data was found. We investigated the potential generated by the anion-radical and the test charge along the line in the direction of the cation-radical. If the chains are orthogonal to each other we are able to model the potential by a point charge placed in a right distance from the line. For the case of the parallel chains the previous claim is no longer valid and we are not able to model the potential considering only the Coulomb interaction of two point charges.

There are several possibilities how to improve the model further. One possibility is to use fitted potential between the anion-radical and the hole to model more precisely the local maximum around the potential well which would improve the quantum yield of free charge carriers photogeneration for the low values of the electric field. By this approach we could also simplify the computation algorithm. Another possibility is to calculate studied problem on a longer model chain. However, the computations time would increased dramatically. We would need to employ different methods of the calculations, because the calculation of much larger system by the DFT method in a reasonable time span is not feasible. One possibility would be to calculate the polymer chain as a periodic system. The problem of this approach is that we are able to solve the optimal geometry of the neutral molecule, but calculating the optimal geometries of the anion-radical and the cation-radical would not be possible. We would have to assume that the geometry of the radicals is the same as of the neutral molecule. Another drawback of our model is how we searched for the mutual position of the adjacent chains. Ideally we should include the changes of the geometry due to the interaction between the chains. This is another thing which should be investigated, too.

An open question is the temperature dependence of the parameters of the model and the application of the model to fitting the temperature dependence of the quantum yield of the charge carrier photogeneration for different temperatures. Unfortunately, for such study the experimental data are not yet available.

Bibliography

[1] Arkhipov V.I., Emelianova E.V., Bässler H.: *Dopant-assisted carrier photogeneration in conjugated polymers*, Chem. Phys. Lett. 372 (2003), 886-892

[2] Menšík M., Pfleger J., Rybak A., Jung J., Ulański J., Halašová K., Vohlídal J.: *Photogeneration of free charge carriers in tenuously packed π conjugated polymer chains*, Pol. Adv. Technol. 22 (2010), 2075-2083

[3] Menšík M., Jex M., Pfleger J., Jung J.: *Photogeneration of free charge carriers in π-conjugated polymers with bulky side groups*, Chem. Phys. 404 (2012), 48-55

[4] Cimrová V.: *Fotogenerace nosičů náboje v polymerech*, Doctorate thesis, Czechoslovak Academy of Sciences (1991)

[5] Silinsh E.A., Kolesnikov V.A., Muzikante I.J., Balode D.R.: *On Charge Carrier Photogeneration Mechanisms in Organic Molecular Crystals*, Phys. Stat. Sci. 113 (1982), 373-393

[6] Knights J.C., Davis E.A.: *Photogeneration of charge carriers in amorphous selenium*, J.Phys.Chem.Solids 35 (1974), 543-554

[7] Noolandi J., Hong K.M.: *Theory of photogeneration and fluorescence quenching*, J.Chem.Phys. 70 (1979), 3230-3236

[8] Szabo A., Ostlund N.S.: *Modern Quantum chemistry*, Dower Publication Inc. (1996)

[9] Skála L.: *Kvantová teorie molekul*, Karolinum (1994)

[10] Becke A.D.: *Density-functional thermochemistry. III. The role of exact exchange*, J. Chem. Phys. 98 (1993), 5648-5652.

[11] Lee C., Yang W., Parr R.G.: *Development of the Colle-Salvetti correlation-energy formula into a functional of the electron density*, Phys. Rev. B 37 (1988), 785-789.

[12] Toman P., Nešpůrek S., Jang J.W., Lee C.E.: *Conformation changes of polysilanes during the polaron formation*, Curr. App. Phys. 2 (2002), 327-330.

[13] Toman P., Bartkowiak W., Nešpůrek S., Sworakowski J., Zaleśny R.: *Quantum-chemical insight into the design of molecular optoelectrical switch*, Chem. Phys. 316 (2005), 267-278.

[14] Toman P., Nešpůrek S., Yakushi K.: *Electronic states and infrared spectroscopy of Ni- and Co-phthalocyanines: neutral and oxidized forms*, J. Porphyrins Phtalocyanines 6 (2002), 556-562.

[15] Toman P., Nešpůrek S., Jang J.W., Lee C.E.: *Oligo[methyl(phenyl)-silane] ion-radical conformations calculated by the B3LYP method*, Int. J. Quantum Chem. 101 (2005), 746-752.

[16] Frisch M.J., Trucks G.W., Schlegel H.B., Scuseria G.E., Robb M.A., Cheeseman J.R., Scalmani G., Barone V., Mennucci B., Petersson G.A., Nakatsuji H., Caricato M., Li X., Hratchian H.P., Izmaylov A.F., Bloino J., Zheng G., Sonnenberg J.L., Hada M., Ehara M., Toyota K., Fukuda R., Hasegawa J., Ishida M., Nakajima T., Honda Y., Kitao O., Nakai H., Vreven T., Montgomery Jr. J.A., Peralta J.E., Ogliaro F., Bearpark M., Heyd J.J., Brothers E., Kudin K.N., Staroverov V.N., Kobayashi R., Normand J., Raghavachari K., Rendell A., Burant J.C., Iyengar S.S., Tomasi J., Cossi M., Rega N., Millam J.M., Klene M., Knox J.E., Cross J.B., Bakken V., Adamo C., Jaramillo J., Gomperts R., Stratmann R.E., Yazyev O., Austin A.J., Cammi R., Pomelli C., Ochterski J.W., Martin R.L., Morokuma K., Zakrzewski V.G., Voth G.A., Salvador P., Dannenberg J.J., Dapprich S., Daniels A.D., Farkas Ö., Foresman J.B., Ortiz J.V., Cioslowski J., Fox D.J.: *Gaussian 09*, Revision C.01, Gaussian, Inc., Wallingford CT (2009)

[17] Hariharan P.C., Pople J.A.: *The influence of polarization functions on molecular orbital hydrogenation energies*, Theoret. Chimica Acta 28 (1973), 213-222

[18] Francl M.M., Pietrol W.J., Hehre W.J., Binkley J.S., Gordon M.S., DeFrees D.J., Pople J.A.: *Self-consistent molecular orbital methods. XXIII. A polarization-type basis set for second-row elements* , J. Chem. Phys. 77 (1982), 3654-3665

[19] Grimme S.: *Semiempirical GGA-Type Density Functional Constructed with a Long-Range Dispersion Correction*, J. Comput. Chem. 27 (2006), 1787-1799

[20] Mohr P.J., Taylor B.N., Newell D.B.: *CODATA Recommended Values of the Fundamental Physical Constants: 2006*, Rev. Mod. Phys. 80 (2008), 633-730

[21] Wolfram Research, Inc.: *Mathematica*, Version 8.0, Champaign, IL (2010)

[22] Newtom M.D.: *Quantum Chemical Probes of electron-Transfer Kinetics: The Nature of Donor-Acceptor Interactions*, Chem. Rev. 91 (1991), 767-792

[23] Grozema F.C., van Duijnen P.Th., Berlin Y.A., Ratner M.A., Siebbeles L.D.A.: *Intramolecular Charge Transport along Isolated Chains of Conjugated Polymers: Effect of Torsional Disorder and Polymerization Defects*, J. Phys. Chem. B 106 (2002), 7791-7795